Chapter - 3

Copper Oxide Thin Films: Growth Mechanism, Properties and Applications towards Catalyst and Sensors

Controlled thermal oxidations of thin copper films leading towards the formation of a single copper oxide phase are investigated, where the oxidation temperature, duration, oxygen partial pressure, film thickness and the crystallographic orientations play very crucial roles to significantly control the final oxide phase of the copper films. Thin Cu films of various thicknesses (100-1000 nm) were deposited on glass and silicon substrates, using a vacuum assisted thermal evaporation technique. Oxidations of these thin Cu films were performed at different temperatures for variable durations in air as well as oxygen ambient conditions. X-ray diffraction (XRD), Four probe resistivity measurement, scanning electron microscopy (SEM), X-ray photoemission spectroscopy (XPS), Raman spectroscopy, ultraviolet-visible (UV-Vis) spectroscopy, atomic force microscopy (AFM) and scanning tunneling microscopy (STM) techniques have been used for the characterization of oxidation mechanism of thin Cu thin films.

At a thermodynamic equilibrium, it has been observed that the oxide phase is solely determined by the oxidation temperature. The initial oxidation of the copper films starts at about 150°C, but a well ordered crystalline phase of the cuprous oxide (Cu_2O) is observed only above 200°C in air ambient condition. However, the cupric oxide (CuO) phase starts to appear above 320°C. At thermodynamic equilibrium, the completion of the oxidation process is mostly controlled by the diffusion kinetics, which further depends on the thickness of initial Cu layers. In addition, the oxide phase is also found to be highly sensitive to the oxygen partial pressure. In compare to air oxidation, under O_2 ambient condition oxidation process occurs at relatively lower temperatures. Single crystalline Cu_2O phase starts to format about 150°C whereas the CuO phase starts to appear only above 260 °C. A strong asymmetry in oxide growth has also been observed leading towards the formation of CuO nano-rods. Significantly lower oxidation

temperatures (for O_2 ambient) have been explained in terms of oxygen partial pressure which significantly enhances the chemical reactivity of the copper atoms with the oxygen molecules as well as further facilitates the oxygen diffusion process through the copper layer.

In one hand, nano-structured Cu_2O thin film having a homogeneous surface morphology with tiny faceted structures exhibited a high photo-catalytic activity showing the degradation of industrial pollutant such as methylene blue (MB) under the visible light irradiation. Under an optimum condition, degradation rate of MB can be reached over 98% in 15min. where the MB molecules completely decomposed into bio-friendly materials.

On other hand, nano-structured CuO thin films have been used as an active layer for CO gas sensors with high sensitivity at relatively low operating temperature. The operating temperatures can be reached as low as 150°C for a CO concentration down to 25 ppm with fast response and recovery times as well as good reproducibility. Among different oxide films, CuO nanostructures grown at lower oxidation temperature (350°C) has been found to be more efficient for CO sensitivity, which can be explained in terms of relatively rough surface morphology as well as temperature dependent unintentional Cu vacancy within CuO leading towards a p-type nature of the semiconducting film. Finally, a correlation between various analytical properties of CuO films and their CO sensing abilities has also been discussed.

3.1 INTRODUCTION

Understanding of the oxidation process of metal thin films is of fundamental as well as high practical interest due to their environmental stability as well as for further processing of metal oxide based semiconductor nanostructures. From thermodynamically point of view, almost all the metals are having a tendency to be oxidized. The driving force behind the oxidation process of a given material depends on change in Gibbs free-energy due to oxide formation at that temperature. In general, thermal oxidation is a complex chemical process, where oxides are grown in an oxidant ambient at elevated temperatures. The simplest form of thermal oxidation of a metal surface may occur even at room temperature, when the film is exposed to oxygen or air ambient and a thin layer of native oxide is spontaneously formed. Afterwards, the oxide growth slows down and effectively stops within a few nanometers because of too little energy of the oxygen atoms to diffuse through the already formed native oxide layer at room temperature. However, thermal oxidation of metal films at an elevated temperature may significantly be controlled by the oxygen atoms diffusion process and their chemical reactivity with the metal atoms. More precisely, the oxidation process is strongly influenced by the physical ambient such as temperature [1], duration, oxidant's partial pressure [2] as well as the film thickness [3] and their crystallographic orientations [4].

The exact oxidation kinetics of metals at nanometer scale also provides fascinating scientific information, which can be a demanding part of the rapidly growing field of nano-science and nano-technology. The controlled growth mechanism through surface processing may also lead to the formation of self-assembled ordered nanostructures of various shape, size and distribution (nano-dots [5], nano-wires [6], nano-wells [7]), having very specific properties such as quantum confinements. Hence, controlled formation of oxide nanostructures would also be technologically very important for their potentially novel optical, electronic, magnetic and sensor properties. Therefore, surface oxidation may act as a processing tool for creating self-ordered semiconductor nanostructures, where a proper understanding of the oxidation mechanism will provide the essential insights into the complex growth kinetics of nano-scale oxide formation.

In recent years, copper oxides (CuO_x) based nano-materials have gained more attention in the field of gas sensor and photo-catalysis and solar energy conversion, due

to their remarkable material properties. Basically, copper oxides are of two principal types such as cuprous oxide (Cu_2O, cuprite) and cupric oxide (CuO, tenorite). In general, Cu_2O appears red in colour as it absorbs visible light in this wavelength range. However, CuO usually appears in black or grey colour which exhibits an indirect band gap. Optical photographs of both type of copper oxide thin films are depicted in Figure 3.1. More details about both copper oxides (Cu_2O and CuO) are already discussed in Chapter 1. Two major applications of these copper oxides films such as photo-catalytic dye degradation using Cu_2O and carbon monoxide sensing using CuO are briefly discussed in the following.

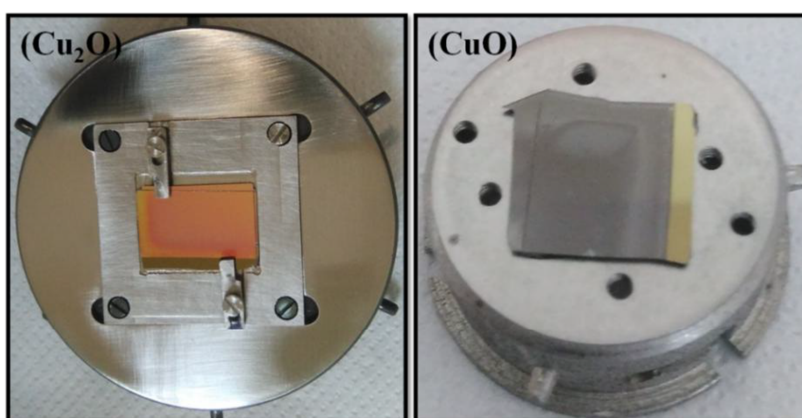

Figure 3.1: *Optical photographs of (a) cuprous oxide and (b) cupric oxide thin films grown on glass substrates.*

Photo catalysis and dye degradation: It is one of the main chemical routes for the successful destruction of environmental toxic pollutants. In addition, photon induced water splitting leading towards the hydrogen production would also be one of the most exciting challenges for renewable energy sources. Nano-materials [8] and nano-composites based metal oxides [9] exhibit a good absorption in the visible light wavelength region due to their suitable band gap. The size dependent optical properties of the nano-materials and nano-composites promote their use as photo-catalytic agent in the various processes like dye degradation of industrial effluents, antimicrobial activity, H_2 evolution from water splitting [10] etc. Specially, organic dyes are one of the major groups of pollutants in waste waters. Hence, this environmental problem associated with hazardous wastes and toxic water pollutants demands a proper recycling process where metal-oxide based nano-materials can be potential candidate.

In general, metal oxide based nano-materials have a wide range of applications oriented with photo catalysis based recycling in textile industries, optoelectronic based energy resources, medical, and other industrial areas. Among the various metal oxide semiconductors, Cu_2O is playing an important role as photo catalysts in environmental application [11 -12]. MB (heterocyclic aromatic chemical compound with molecular formula ($C_{16}H_{18}ClN_3S$) is one of the most common dyes used in the textile industries. This dye is stable and incompatible with bases, reducing agents and strong oxidizing agents. During a chemical or biological reaction pathway, these dye compounds not only deplete the dissolved oxygen in water bodies but also release some toxic compounds to endanger aquatic life [12]. However, to overcome this issue, a photo-catalytic dye-degradation process will be one of the most attractive as well as cost-effective approach for waste water remediation. It has already been reported that MB can be photo-degraded under visible light irradiation on a proper choice of catalyst [13-14].

CO sensing within the limit of tolerance: Carbon monoxide (CO) is known as one of the most poisonous gas, 'a silent killer', because it is colorless, odorless, tasteless and non-irritating. Hence, it is very difficult to detect CO by our human sensors. Breathing in the carbon monoxide environment over long periods of time can cause headache, unconscious, dizziness, vomiting, increased risk of heart disease and even death. For a very low concentration of CO such as 30 ppm may also cause severe health issues, for a long duration of inhalation. Therefore, an early detection of low concentration CO is of high importance. In general, carbon monoxide concentrations are particularly higher in the industrial areas [15]. However, many common devices can also produce significant amount of carbon monoxide, which include cars, gas appliances, wood stoves as well as cigarettes. According to the United States National Institute of Occupational Safety and Health (NIOSH), 35 ppm of CO exposure over 8 hrs period is the maximum time weighted average exposure for survival of a human body [16]. In the case of the concentration of CO gas as low as 20-30 ppm, for several hours' exposure can also affect the human health in an unrecoverable manner. Hence, a proper precaution against any carbon monoxide exposure such as a low concentration CO sensor is highly desirable. Therefore, highly sensitive CO sensors which can work at a relatively lower operating temperature are of high practical demand. In this aspect, CuO based nano-structured this films can be a potential candidate.

All these above mentioned phenomena clearly indicate that the oxide phase purity of the copper film can be an important issue towards its application in catalyst or sensor devices. Various growth techniques have been employed for device quality copper oxides formation such as, sol-gel process [17], spray pyrolysis [18], solution growth [19], chemical vapour deposition (CVD) [20], pulsed laser deposition (PLD) [21] and DC and RF magnetron sputtering [22 - 25], molecular beam epitaxy (MBE) [26], anodic and chemical oxidations [27 - 28], and electrochemical deposition [29 - 31]. These growth techniques generally require some special growth conditions, however, still results in a mixed oxide phases. Hence, formation of a single oxide phase of Cu thin films is of high practical importance for photo catalytic and gas sensor devices applications.

So far, chemical growth routes were mostly followed to grow the copper oxide nano-structures, where the material's purity could be a critical issue due to the possibilities of any unintentional contamination. However, vacuum assisted physical vapor deposition (PVD) growth of oxide material under cleaner ambient through physical route would be an alternative approach [4 - 32]. Within this work, a simple and efficient approach, vacuum assisted evaporation of thin metal films followed by controlled thermal oxidation (up to 600°C) has been used to form a single phase of copper oxides. A systematic study of the oxidation mechanism and temperature dependent diffusion process of the oxidizing species leading towards the oxide phase transition have been investigated. Finally, these copper oxides (CuO_x) nano-structured thin films are used towards the application of CO gas sensing and photo-catalytic dye degradation process.

3.2 EXPERIMENTAL DETAILS

Thin copper films of various thicknesses (100nm - 1000nm) were deposited at room temperature on glass and silicon substrates, using the vacuum assisted thermal evaporation technique. All substrates were ultrasonically cleaned with acetone, isopropanol, and methanol for about 15 minutes followed by drying with pure nitrogen gas, prior to loading into the vacuum chamber. During Cu deposition, the chamber pressure remained in the range of $\sim 10^{-5}$ mbar and the evaporation rate was maintained about ~3 Å/sec to have uniform and homogeneous films. The as-grown copper films

were then thermally oxidized in air as well as under an oxygen ambient condition at different atmospheric pressures. The oxidation temperatures were varied in a wide range from room temperature (RT) to 600°C, in a precisely controlled manner. A slow cooling rate of $< 10°C / min$ was preferred to minimize the possible thermal stress and improve the crystalline quality of the oxide films.

All copper oxides films were afterwards characterized for structural, morphological, electrical, chemical and optical properties using various analytical techniques. To investigate the initial oxidation of Cu films, sheet resistance of the thin Cu films was measured by the four point probes technique with a probe-spacing of 2 mm, using the Physical Quantity Measurement System (PQMS) from Qazartech. The crystallographic structures of the oxide films were investigated by Rigaku Mini Flux II X-ray diffractometer (XRD) with Cu-Kα radiation (λ = 1.54 Å).The surface morphology of the copper oxide films was analyzed with a commercial field emission scanning electron microscopy (FESEM) from Nova NanoSem 450, operated from 0.5 to 30 kV. In addition, the surface topography of copper oxide thin films was investigated using atomic force microscopy (AFM). Scanning tunneling microscopy (STM) is used for to investigate the nm scale surface textures and their electronic states. Optical transmittance of the oxide films was recorded using a Simazu UV-visible optical spectroscopy within the wavelength range of 300-800 cm^{-1}. Raman spectroscopy measurements were also performed to distinguish the oxide phases of the films, using a commercial Raman unit from Horiba Scientific. Finally, X-ray photoemission spectroscopy (XPS) measurement was performed to find the oxidation states of Cu and the phase purity of the copper oxides layer. During XPS measurements, the base pressure of the chamber was maintained below $< 10^{-9}$ mBar and monochromatic Al K_{α} (1486.6 eV) and Mg K_{α} (1256.7 eV) lines were used as X-ray sources. All binding energies of the emitted photoelectrons are calibrated to the C1s binding energy at 284.5 eV.

3.3 RESULTS AND DISCUSSION

Controlled Growth of single oxide phase of copper films was influenced by many parameters such as ambient conditions, oxidation temperature, duration of annealing, oxygen partial pressure, film thickness and crystallographic orientations. Details studies of these parameters are discussed in the following.

3.3.1 Oxidation Process of Thin Copper films

Within this section, how the oxidation temperature and duration can significantly influence the oxidation process of thin Cu film have been discussed and explained in terms of thermodynamic, Gibbs free energy and diffusion kinetics. In addition, effect of O_2 partial pressure as well as crystal orientation has also been discussed. Finally, a schematic model for temperature dependent thermal oxidation process of thin Cu film is also proposed.

3.3.1.1 Initial oxidation

Four probe resistivity measurement techniques have been employed here to find the temperature required for the initial oxidation process of the Cu films. A schematic of the sheet resistance (R_s) measurement is already mentioned earlier in Chapter 2. To measure the sheet resistance of the Cu films, outer two probes were used as current (I) source whereas the inner two were used to measure the voltage drop (V) across the surface. To find the initial oxidation of the Cu film surface occurred during air annealing, the surface resistance of the Cu film has been monitored. During measurement, samples were annealed in air as well as helium ambient within a metal tube, equipped with a cylindrical heater. A silicon diode was used to measure the sample temperature (uncertainty of ±10°C). It is important to mention that the annealing temperature rises almost linearly with a heating rate of 2°C/ min from room temperature up to 130°C. Afterwards, the heating rate was lowered for better precision and observed to be 0.15°C/ min during the last 20°C of annealing. In Figure 3.2(a), temperature dependent sheet resistances of the Cu films in air ambient are depicted where the increase in sheet resistance (Rs) with the annealing temperature (T) is shown. A linear increase in resistance with annealing temperature (T) has been observed for temperature up to 140°C. This constant slope of in R-T plot can be related to the thermal coefficient of resistivity of the Cu film. However, a sudden increase / jump in sheet resistance are observed above 140°C, which indicates the onset of surface oxidation of the Cu film at this particular temperature.

For further confirmation of the initial surface oxidation process of Cu film during annealing in air above 140°C, R-T measurements with heating and cooling cycles have

been performed on a Cu film, firstly in a helium ambient condition followed by an air ambient. Both R-T plots with heating and cooling cycles are depicted within Figure 3.2(c). In case of the ambient annealing, the R-T plot linearly increases up to 150°C without any jump / sudden increase in sheet resistance. In addition, the cooling cycle almost follows the heating path indicating no such chemical changes (oxidation) of the film surface during the annealing under Helium (He) ambient condition. Whereas, for air ambient annealing, same sample shows a rapid increase in sheet resistance just above 140 °C. Moreover, the cooing path follows the heating slope but with a constant upward shift due the onset surface oxide formation above 140°C.

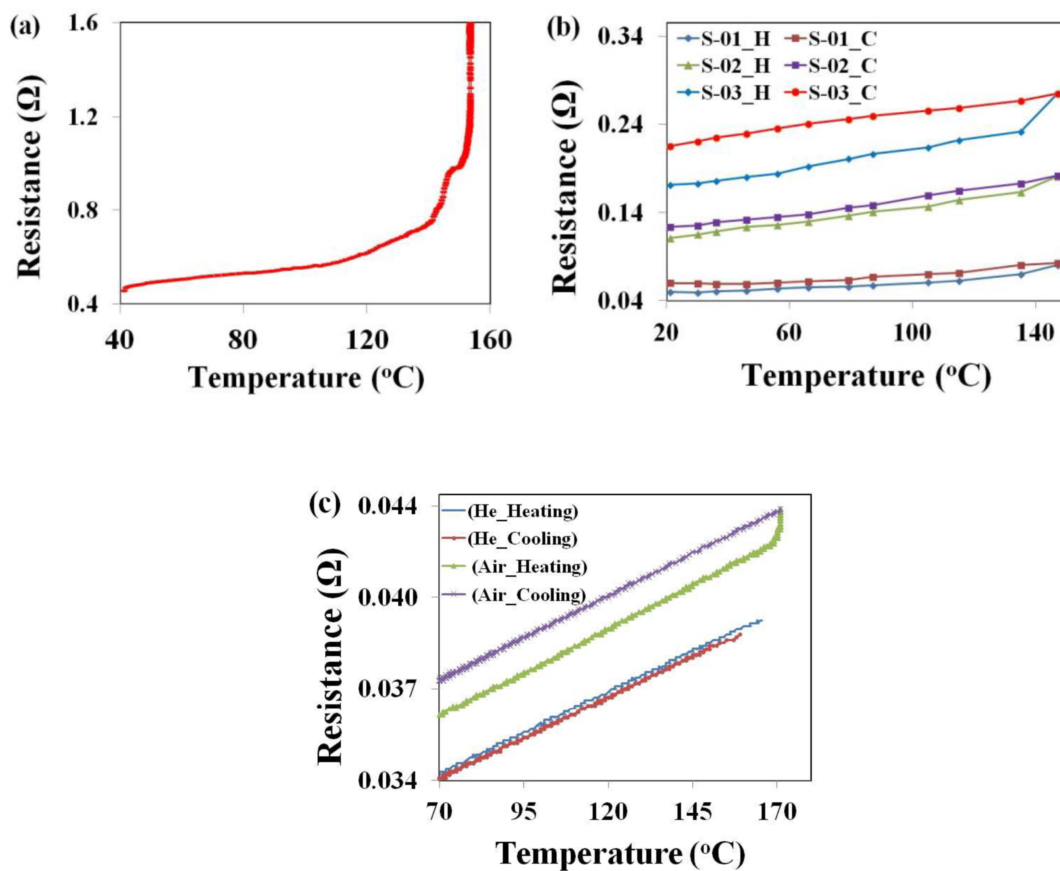

Figure 3.2: *Thin Cu films show (a) Temperature dependent sheet resistance in air, (b) R-T measurements of heating and cooling cycles of different Cu films during air annealing (c) comparison of sheet resistance during heating and cooling cycles in air as well as He ambient conditions.*

To avoid any kind of uncertainty, similar resistivity measurements of the heating and cooling cycles have also been performed for different Cu films, as can be seen within

Figure 3.2(b). To have a better statistics and minimize any kind of contact errors, all I-V data was recorded here at a particular temperature and the corresponding slope was then measured to plot the R-T data here. The linear increase in resistance with annealing temperature having a constant slope related to the thermal coefficient of resistivity is also followed. Both the heating and cooling lines show almost identical slopes. In addition, a minor vertical shift in sheet resistance for the cooling line as compared to that of the heating is recorded in each case. This could due to be the fact that the oxide layer formation starts on Cu surface only above 140°C, during annealing in air ambient condition [32-33]. In the Figure 3.2 (b), it is clearely observed that the sample S-03 is having a slightly higher variation in sheet resistance duing the cooling cycle as compare to other two samples (S-01 and S-02) which can be explain in terms of the thickness effects and early oxidation. Samples S-01 and S-02 have slightly higher thickness of ~ 600 nm, whereas sample S-03 has a lower thickness of ~200 nm. It is already reported in various literatures that thinner films get easily oxidized as compare to the thicker films at a particular oxidation temperature and hence, S-03 oxidizes earlier than others.

From all the above findings we can conclude that thermal oxidation of the copper film in air starts at about 140°C which can be explained in the following way. Spontaneous formation of a very thin native oxide layer on copper film is quite obvious at room temperature as soon as it is exposed to air. Afterwards, this native oxide layer acts as a barrier for further oxidation of the Cu film by limiting the diffusion of the oxygen molecules through it. As a result, further oxidation of the Cu film is protected at room temperature. However, at about 150°C, thermal energy starts to overcome the diffusion barrier and further oxidation of Cu film starts, which is clearly reflected by a sudden increase in the slope of the R-T plot. A vertical shift in sheet resistance from heating to cooling cycle within the R-T plot also indicates an increase of the sheet resistance by slight thickening of the oxide layer during annealing of the film above 140°C. As the heating rate was quite slow at this temperature range and altogether the duration of annealing above 140°C was more than 30 min, a reasonable amount of surface oxidation may be expected, which further reflects the change in the sheet resistance as well a film color [4, 33]. A similar kind of jump in bulk resistivity for Cu film has also been reported by *Valladares et. al.* after an air oxidation [32-33].

3.3.1.2 Temperature dependent oxide phases and role of thermodynamics

In order to understand the formation of various copper oxide phases, XRD analysis of thin copper films has been performed as a function of oxidation temperature [Figure 3.3]. All films were furnace annealed within a closed chamber in air ambient at different temperatures and durations. As-deposited Cu films show sharp diffraction peaks centered at about at 43.4° and 50.6° (2θ value), attributed to the (111) and (200) reflection planes, respectively (Figure 3.3 (I, a)) [32-34]. Sharp diffraction lines confirm the formation of a well oriented and crystalline Cu film on glass substrate, even after Cu deposition at room temperature. As compared to the reported chemical growth process, the pattern shows only two or three diffraction lines which are also an indication of a preferential growth orientation of the Cu film. Although, earlier sheet resistivity measurements suggest that the oxidation process of the Cu film in air starts at about 150°C, we have not observed any XRD peaks of copper oxides below 250°C. [This ambiguity will be discussed later in subsection 3.3.2 of Raman spectroscopy as well as XPS]. Figure 3.3 (I, b) shows the XRD patterns start to change only after oxidizing the film at a temperature above 250°C. In addition to the Cu diffraction lines, an additional diffraction peak centered at 2θ = 36.4° starts to appear. This peak position represents an inter-planar lattice spacing of d = 2.44 Å which can be attributed to the (111) reflection planes of cubic phase Cu_2O [JCPDS card no.: 05-667, 4, 29, 33]. Figure 3.3 (I, b) represents the XRD patterns of Cu films annealed at 280°C for 3 hours which appears with a new diffraction peak at 2θ = 36.4°. This can be concluded as the initial stage of crystalline Cu_2O phase formation and as a whole, the film exhibits a mixture of Cu and Cu_2O phases. Continuation of the oxidation process at the same temperature will result in an increase of the Cu_2O (111) diffraction peak intensity whereas a decrease in the Cu diffraction peaks and finally the hole Cu film will convert into a crystalline Cu_2O phase, with a strong preferential orientation along (111) lattice plane. Towards the end of the oxidation process, a weak diffraction peak centered at 42.3°, corresponding to Cu_2O (200) starts to appear [32-34]. Further increasing the oxidation temperature does not change the scenario very much except a faster oxidation process. Figure 3.3 (I, c) shows the XRD pattern, after oxidation at 300°C for 3 hours where the additional diffraction peak of Cu_2O (200) has become much stronger. However, we have not seen any trace of CuO formation at this temperature. It

has to be taken into account that XRD in not a very surface sensitive techniques and it may only detect an oxide phase after a significant amount of surface oxidation of the Cu film (~5%) has already been occurred. XRD is not able to detect the very thin and also poor crystalline quality of oxides layer. However, prolonged oxidation (up to 20 hours) at a temperature below 320°C does not show any trace of CuO formation in XRD pattern which successfully excludes the formation of CuO at this temperature.

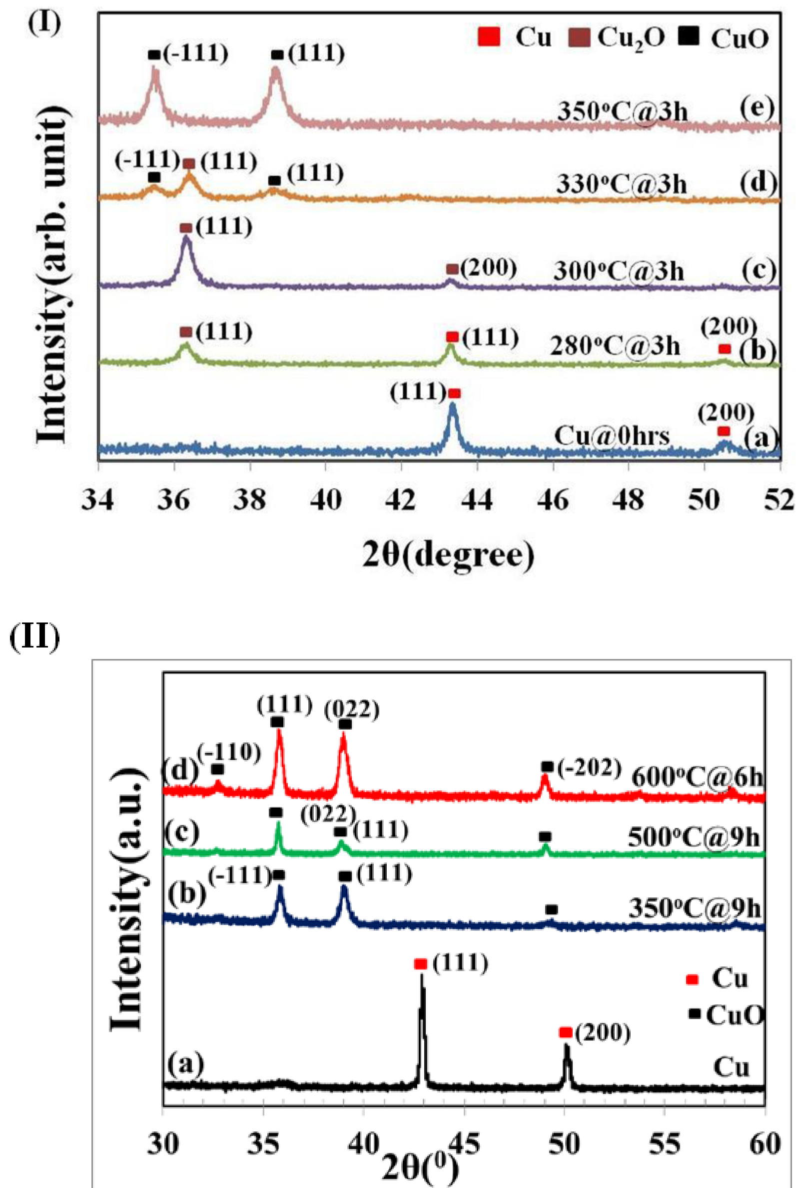

Figure 3.3: *XRD spectra (θ - 2θ scan) of thin Cu films after oxidation in air at various temperatures for (I) RT to 350℃ for 3hrs durations and (II) 350℃ to 600℃ for different durations*

A drastic change in XRD pattern is only found for oxidation above 320°C, as an indication of CuO formation. Two low intensity diffraction peaks centered at 2θ = 35.5° and 38.8° start to appear on either sides of the Cu_2O (111) peak (Figure 3.3 (I, d)). These diffraction lines can be attributed to the (−111) and (111) reflection planes, respectively, of the CuO monoclinic phase [JCPDS cards no.: 45-0937, 4, 32-34]. The film predominantly consists of Cu_2O phase along with a small amount of CuO phase. Continuation of oxidation at this temperature slowly converts the whole film into a crystalline CuO layer at the cost of Cu_2O phase. Further increase in oxidation temperature then the results show a faster oxidation of the film to CuO, as shown in Figure 3.3 (I, e) [350°C for 3 hours].

Oxidation at even higher temperatures (350°C-600°C) for longer duration (6-9 hrs) is depicted in Figure 3.3 (II). The (-111) reflection peak becomes much stronger here and an additional peak is also appeared at 49.6°, which are originated from (-202) reflection planes of CuO film, as shown in Figure 3.3 (II, a-c)) [JCPDS cards no.: 45-0937)]. This additional peak (-202) becomes sharper with increase in oxidation temperature from 350°C to 600°C. After annealing at 500°C for 9hrs in air, a drastic change in XRD pattern has been observed. Two additional diffraction peaks appeared at 33.28° and 49.58° which are originated from (002) and (100) reflection planes of CuO film, respectively [Figure 3.3 (II, c)]. Increase in oxidation temperature of about 600°C for 6hrs results in two strong oxide peaks of (002) and (101) reflection planes of CuO [Figure 3.3 (II, d)] [33, 35]. However, at these oxidation temperatures, no traces of copper and cuprous oxide are found in XRD.

From all these above findings it can be concluded that the oxide phase of the Cu film is strictly determined by the oxidation temperature, which can further be explained in terms of chemical activation energy of the oxide phase formation. Gibb's free energy change (ΔG) for chemical reaction is determined by the changes in enthalpy (ΔH), entropy (ΔS) and the absolute temperature (T) as:

$$\Delta G = \Delta H - T(\Delta S)$$

where, an increase in absolute temperature T results in a decrease in the ΔG value. A reaction can be spontaneous only if the value of the free energy (ΔG) becomes

negative. Hence, the onset of native oxide (Cu_2O) formation at room temperature, during exposure of the Cu film to air, indicates that the value of ΔG is negative for Cu_2O formation. However, the oxidation process was mainly restricted by the diffusion kinetics of the O_2 through the surface oxide layer. With increase in temperature, thermal energy helps to overcome the diffusion barrier as oxidation proceeds. But there was no trace of CuO formation below 320°C, even for a long duration (20 hours) of oxidation as the diffusion kinetics does not play any significant role here. Therefore, it is expected that at lower temperature the value of ΔG is to be positive in case of CuO formation, which turns to a negative value when the temperature exceeds 320°C and as a result it overcome the chemical reaction barrier. Moreover, even after oxidation for sufficiently long duration (*i.e.* under thermodynamic equilibrium) we have not seen any coexistence of CuO with the metallic Cu phases. This finding also confirms that at thermodynamic equilibrium oxide phase is solely determined by the oxidation temperature, not by the growth kinetics. Finally, for both Cu oxides, increase in temperature enhances the diffusion kinetics of the O_2 and as a result a faster oxidation occurs. Therefore, it can be concluded that at thermodynamic equilibrium copper oxide formation by thermal oxidation follows the phase sequence of Cu → (Cu + Cu_2O) → Cu_2O → (Cu_2O + CuO) → CuO, where pure Cu_2O phase occurs for a small window of annealing temperature between 250°C and 320°C. A similar kind of copper oxide phase evolution with oxidation temperature has also been reported [4, 32-34, 36].

Apart from the evolution of different copper oxide phases at various oxidation temperatures, the average crystallite size of these oxide films have also been estimated. *Debye-Scherrer formula* has been used to calculate the average grain/crystallite size of all oxide phases using different XRD peaks as follows:

$$D= (0.91\ \lambda) / (\beta\ Cos\theta)$$

where λ is the wave length of X-ray (0.1541 nm), β is the full width at half maximum (FWHM) in radian, θ is the diffraction angle, and D is the particle diameter [37]. A comparison of the average grain sizes of different CuO_x films is summarized in Table 3.1 and Figure 3.5. A clear decrease in grain size from Cu → Cu_2O → CuO has clearly been observed for lower oxidation temperature (Table 3.1). This finding will be explained in the following way as shown in Figure 3.4.

In general, the nucleation of Cu_2O is initiated at the crystal defects sites of Cu. Oxidation below 320°C expands the Cu_2O nanocrystals/grains within the Cu grain, forming new grain boundaries of Cu_2O. However, within this temperature range, a higher oxidation temperature may result in a relatively larger grain size of Cu_2O. Future increase in oxidation temperature (above 330°C) can initiate the CuO formation within a single grain of Cu_2O. A similar mechanism can also be followed during Cu_2O conversion into CuO phase. Hence, a relative grain size distribution of Cu > Cu_2O > CuO can be expected through surface oxidation of thin Cu films.

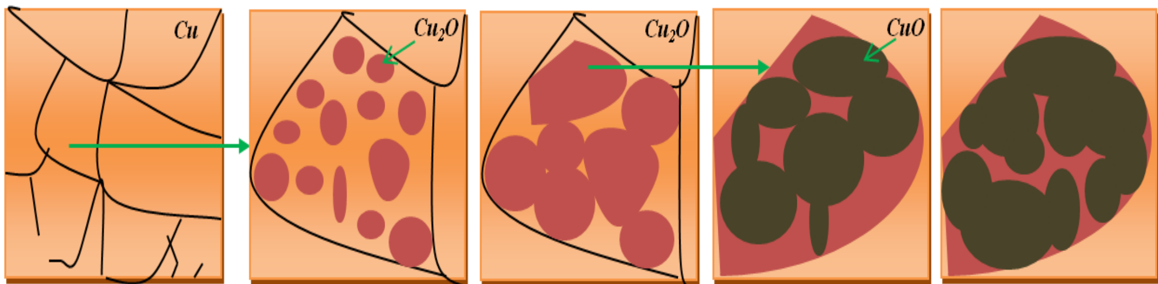

Figure 3.4: *Schematic representation of grain growth during the oxidation of copper thin films.*

Material Details	Oxidation temperature	Crystallite size (nm)
Cu	Room Temp.	41
Cu_2O	350°C for 3hrs	24
CuO	400°C for 3hrs	16

Table 3.1: *Average grain size of thin CuO_x films for different oxide phase.*

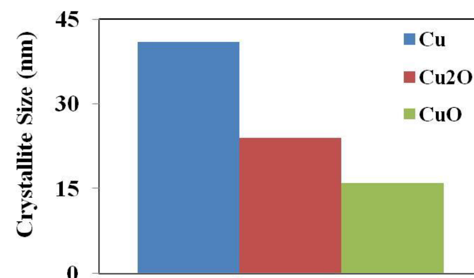

Figure 3.5: *Crystallite size of CuO_x thin films for different oxide phase.*

However, a steady increase in CuO crystallite size with oxidation temperature is also noticed [Figure 3.6 and Table 3.2]. This gradual increase in average grain size can be explained in terms higher surface diffusion. At a lower oxidation temperature of 350°C, multiple nucleation sites of CuO phase start to form within a single Cu_2O grain as an initial stage of CuO formation, which further coalescence at higher temperature to a larger grain [4, 33]. The above theory can only explain the oxide growth at elevated

temperature as it does not include any terminal cases of oxidation process at room temperature as well as higher oxidation temperature. Here, we will explain the terminal cases of oxidation process in terms of chemical activation energy as well as thermal diffusion of O_2 and Cu species. In one hand, the oxidation of Cu films at room temperature terminates within the native oxide layer of few nanometers thickness which can be explained in the following manner. The native oxide layer acts as a diffusion barrier for O_2 and Cu species at room temperature and plays a preventive role against any further oxidation of Cu film and by restricting the diffusion process. In addition, limited chemical activation energy at room temperature also restricts the further Cu_2O growth in this *reaction-limited* growth regime. As the oxidation temperature increased, diffusion energy also increases and starts to overcome the native oxide barrier at about 150°C. As a result, further oxidation of the Cu film continues. On other hand, oxidation of Cu films at elevated temperature also terminates to its saturation thickness with a thick oxide layer. As the oxide layer gets thicker it drastically reduces the diffusion process of O_2 and Cu species. As a result, oxide growth rate slows down significantly in this *diffusion-limited* growth regime and finally terminates. Therefore, the final oxide layer thickness limits to the saturation thickness which is mostly determined by the oxidation temperature not by the duration of oxidation [4, 33].

3.3.1.3 Effect of diffusion kinetics

Within the limit of chemical activation energy, temperature induced thermal diffusion process of O_2 molecules leading towards the change of oxide phase ($Cu \rightarrow Cu_2O$ and $Cu_2O \rightarrow CuO$) are discussed here. XRD intensity profiles are intensively used here for quantitative analysis of the oxide growth as a function of oxidation time. Starting from the metallic Cu films, their stepwise oxidations at 260°C and 300°C up to the completion of Cu_2O phase, depends on the duration of oxidation as depicted in Figure 3.7(a and b), respectively. The XRD patterns of the initial Cu film appear with strong diffraction peak at $2\theta = 43.4°$, originating from the Cu (111) reflection planes. With duration, the oxide phase starts to become visible at $2\theta = 36.4°$, representing the (111) lattice planes of Cu_2O phase. This peak gets stronger at the cost of Cu (111) peak intensity, following domination over the metallic Cu phase, and finally completes to the pure Cu_2O phase. Moreover, an additional diffraction peak at $2\theta = 42.3°$ attributed

to the (200) reflection planes of Cu_2O has also been observed towards the completion of the oxide phase. However, it is quite clear from the comparison of both the XRD patterns that the Cu_2O oxidation process is much faster at 300°C as compared to that of 260°C. A quantitative analysis of the oxide growth at 260°C and 300°C, as a function of oxidation time, is depicted in Figure 3.7(c - f).

Oxidation temp. for 3hrs	Crystallite size (nm)
300 °C	14
350 °C	16
400 °C	17
450 °C	18
500 °C	19
550 °C	20
600 °C	21

Table 3.2: *Average grain size of thin CuO films after oxidation at different temperatures in air for 3 hours.*

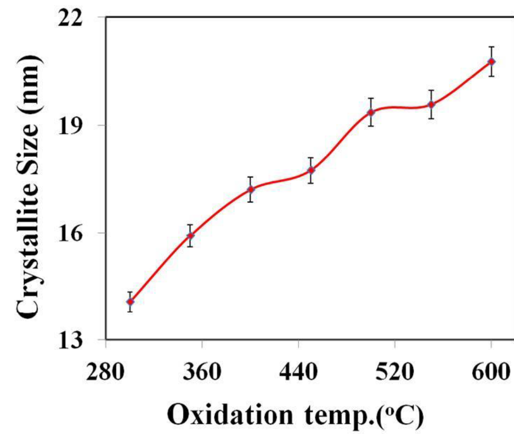

Figure 3.6: *Crystallite size of CuO thin films with oxidation temperatures.*

To determine the amount of remaining metallic Cu as well as the amount of Cu_2O grown through surface oxidation process, a Lorentzian profile has been fitted to the data of the Cu (11) and Cu_2O (111) peaks and displayed in Figure 3.7 (c & d) and Figure 3.7(e & f), respectively. A gradual decrease in Cu (111) peak intensities as well as a gentle increase in Cu_2O (111) peak intensities with the oxidation timing are clearly depicted in Figure 3.7(c & d) and Figure 3.7 (e & f), respectively. Assuming a homogeneous lateral growth of Cu_2O through the surface diffusion of O_2, an estimated depth profile of Cu or Cu_2O are also summarized within the inset of each intensity diagram. Here, we assume a uniform and homogeneous oxidation for all crystallographic orientations which may not be case for the actual oxidation process. The effect of crystallographic orientation on the oxidation process is briefly discussed later in the section 3.1.6. In general, the oxide growth profiles (presented within the insets) follow an overall parabolic pathway with the duration of oxidation. On the other hand, the Cu (111) peak intensity shows a similar decay with the oxidation time [33]. A careful observation of the oxide growth profiles also suggests that the oxide growth rate is much higher at the initial stage and then slows down with layer thickness and finally

terminates. A relatively broader diffraction peaks for Cu_2O as compared to metallic Cu has been noticed and 36.4° and 38.8°, attributed to the (-111) and (111) diffraction lines of CuO, appear after the first annealing step. With duration, both peaks strengthen at the cost of Cu_2O diffraction lines. Moreover, a relatively broad defection peak is found for CuO in comparison to Cu_2O. In this case, two diffraction peaks centered at $2\theta = 35.5°$ and 38.8°, attributed to the (-111) and (111) diffraction lines of CuO, appear after the first annealing step. With duration, both peaks strengthen at the cost of Cu_2O diffraction lines. Moreover, a relatively broad defection peak is found for CuO in comparison to Cu_2O [33].

Within the phase equilibrium, faster oxidation at higher temperature can be explained in following ways. In case of Cu_2O formation, both the oxidation temperatures 260°C and 300°C are kept below the activation energy for CuO formation (330°C) whereas for CuO formation oxidation temperatures are set well above the critical temperature of 325°C. Hence, for both the cases, O_2 diffusion mechanism plays the key role rather than thermodynamics. An increase in oxidation temperature can drastically enhance the O_2 diffusion process through the oxide layer. Hence, a faster growth of Cu_2O layer at 300°C as compare to 260 °C as well as rapid CuO growth at 350°C as compare to 330°C is quite obvious due to an enhanced diffusion of oxidizing species. The impact of further oxidation of Cu_2O films to CuO layer at temperatures of 330°C and 350°C is shown in Figure 3.8.

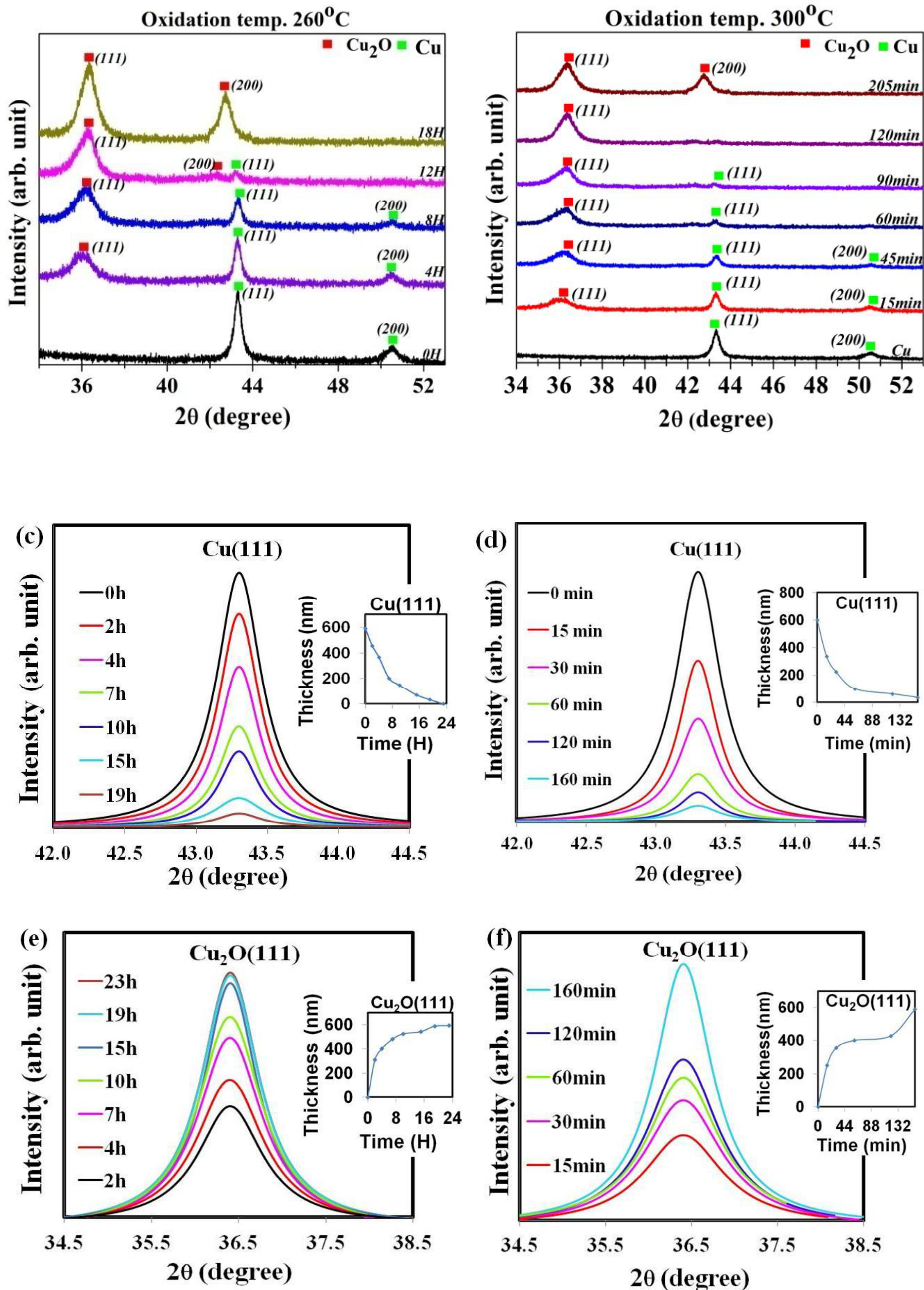

Figure 3.7: *XRD spectra of thin Cu films during evolution of Cu_2O oxide phases after oxidation in air at (a) 260°C and (b) 300°C, for different durations. Lorentzian peak fitting of (c-d) Cu(111) and (e-f) Cu2O (111) diffraction lines, along with their oxide growth kinetics shown within the insets.*

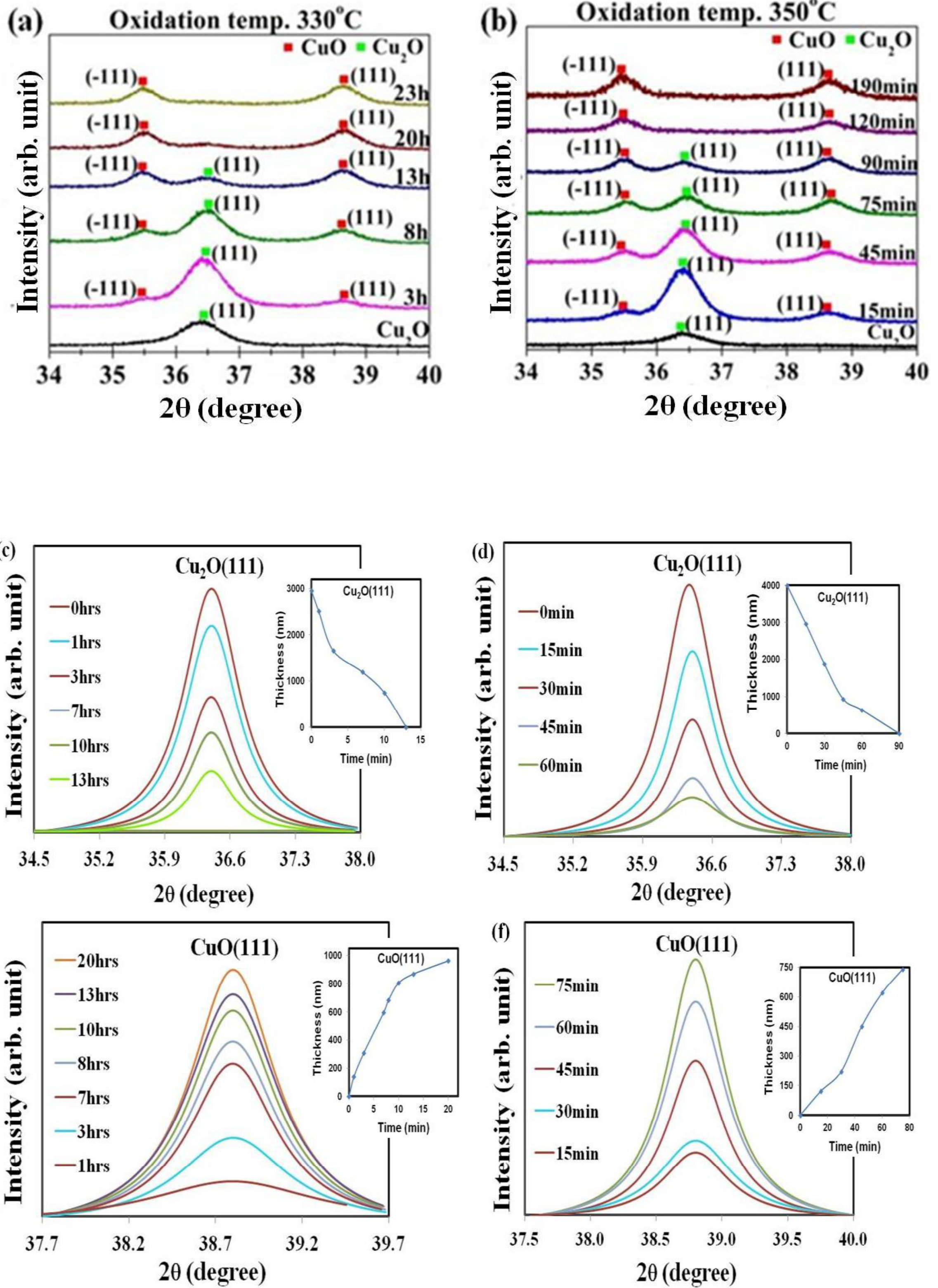

Figure 3.8: *XRD spectra of thin Cu_2O films transformation to CuO oxide phases during thermal oxidation in air at (a) 330°C and (b) 350°C, for different durations. Lorentzian peak fitting of (c-d) Cu_2O (111) and (e-f) CuO (111) diffraction lines.*

3.3.1.4 Interplay between surface kinetic and thermodynamics

Apart from the limit of chemical activation energy and thermal equilibrium conditions, Cu film thickness can also play a crucial role to determine the final oxide phase of the copper film, as shown in Figure 3.9. It is also clearly observed from the XRD results of different copper films that a thinner film (100 nm) oxidizes much faster as compared to a thicker (500nm) film, which can be explained in terms of thermal diffusion of oxygen atoms through the copper surface layer. It is to be noted that here the oxidation was performed under O_2 ambient condition as well as the oxidation temperature (150°C) is much lower as compare to earlier one. The effect of O_2 partial pressure is discussed in the following section. However, XRD results clearly suggest that the oxidation starts from the top of the film surface and slowly diffuse in to the depth of films. This growth mechanism can nicely explain with the findings of Figure 3.9, where a thinner film gets oxidized much faster as compare to a thicker one [33].

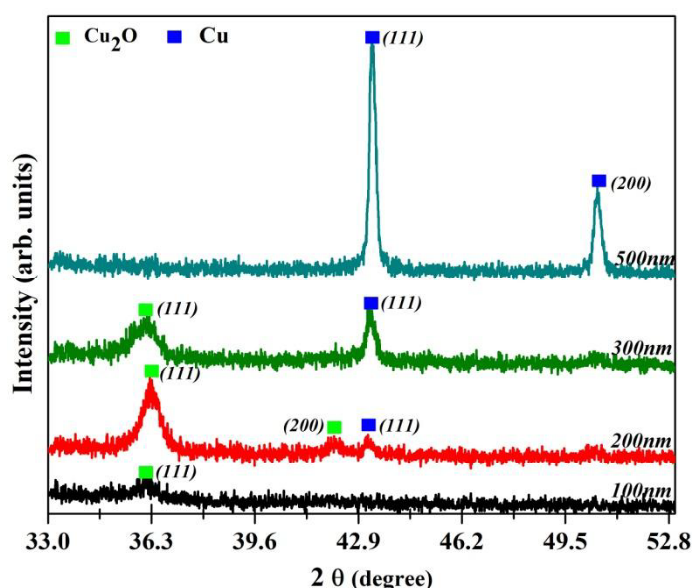

Figure 3.9: *XRD patterns of Cu films of different thickness (100 nm - 300nm) after the oxidation at 150°C for 3hrs.*

The thickness dependent Cu_2O growth rate shown within the insets of Figure 3.7 can be correlated to the following matter. At an early stage of oxidation, the oxide layer is relatively thin. As a result, time taken by the oxidizing species to reach the Cu_2O/Cu interface through diffusion process is much faster than the timescale needed for the chemical reaction to form the Cu_2O. A faster growth rate of oxide film at this initial phase is expected which can be assigned as the *reaction-limited* growth regime. On the

other hand, when the oxide layer becomes thicker, the timescale of diffusion through this layer exceeds the reaction timescale. Therefore, at the later stage the oxidation rate becomes slower and it is assigned as *diffusion-limited* growth regime. More detailed analysis of the diffusion process is discussed in the following.

Diffusive flux (F_1) of the oxidizing species through the Cu_2O over layer to Cu-Cu_2O interface can be represented as $F_1 = D\,(dC/dx) \cong D\,(C_0 - C_s)/x$, where C_0 is the concentration of the oxidizing species in atmosphere adjacent to the film surface, C_s is the concentration of the oxidizing species at the Cu-Cu_2O interface, D is the diffusion coefficient of the oxidizing species, and x is the thickness of the oxide layer. As the reaction rate of the oxidizing species is proportional to C_s, the reactive flux (F_2) can be represented as $F_2 = kC_s$, where k is the reaction rate. In case of initial oxidation within the *reaction limited regime*, the oxidation rate is mainly controlled by the flux rate F_2, whereas for thicker layer of oxide in *diffusion limited regime*, F_1 is the deciding factor of the oxide growth rate. However, in both regimes F_1 and F_2 becomes equal (F) for a steady-state of oxidation and can be represented as $F = DC_0/\,(x+D/k)$, which gives the growth rate of the oxide layer as $dx/dt = Dk\,(C_0/C_1)/(kx + D)$, and C_1 represents the number of oxidizing species per unit oxide volume. The differential equation, with the initial condition of x (t = 0) = 0 yields a generalized quadratic equation:

$$x^2 + Ax - Bt = 0,$$

where, $A = 2Dk$ and $B = 2DC_0/C_1$. Our findings of a parabolic pathway of oxide layer growth with the oxidation time are very much in line with this generalized equation. A very similar kind of oxidation mechanism has also been reported by Dale *et al* for oxidation of silicon surface [31, 33]. However, the minor variation in experimental data may be related to the non-uniform oxidation for the different crystallographic planes.

3.3.1.5 Effect of oxygen partial pressure

To find the effect of oxygen partial pressure, thermal oxidation was carried out by annealing thin copper thin films in a pre-heated horizontal tube furnace under an oxygen ambient condition as well as oxidation with clean O_2 under low vacuum condition (~5×10^{-2} mbar O_2) for different temperatures and durations. As a special interest, how

the O_2 partial pressures can influence the oxidation process and alter the activation temperature of the oxide phase is also tested.

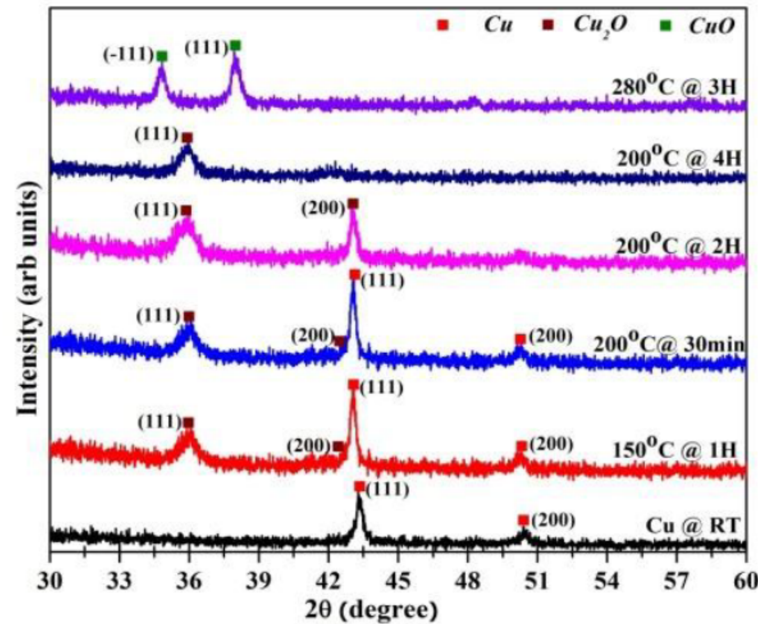

Figure 3.10: *XRD patterns of Cu layers oxidized at oxygen ambient at various temperatures and durations.*

Figure 3.10 shows the XRD spectra of thin Cu films during oxidation at various temperatures and durations under an O_2ambient atmosphere. All oxide films appear in polycrystalline nature with various diffraction peaks which are clearly marked within the Figure. After oxidation of the Cu film at 150°C for 1 hours, sharp diffraction peak at 36.4^o starts to appear which can be related to the (111) diffraction plane of crystalline Cu_2O phase. However, strong existence of Cu (111) and (200) peaks suggests that the Cu film is partially oxidized and a formation of a mixed Cu and Cu_2O phases [Figure 3.9]. By increasing the annealing temperature to 200°C for 30min, the intensity of Cu_2O (111) plane is significantly increased at the cost of Cu (111) and (200) planes. Annealing for longer duration (2 hours) leads to the formation of single phase of Cu_2O which appears at 36.4^o and 42.3^o, correspond to the (111) and (200) planes, respectively. Even longer annealing for 4 hours confirms the formation of single phase Cu_2O with strong reflection from (111) plane. It has been observed that the single phase of Cu_2O is obtained below an oxidation temperature of 260°C. Further increase in annealing temperature (280°C) leads to the XRD peaks at 35.5^o and 38.8^o, correspond to the (-111) and (111) diffraction planes of CuO phase, respectively [33, 38].

A relative comparison of oxidation process under air and O_2 ambient is depicted in Figure 3.11. XRD patterns clearly indicate the crystalline Cu_2O formation starts at 150°C which was not seen for the case of oxidation process in air, even at 250°C. Similarly, oxidation at 280°C under oxygen ambient results in CuO formation instead of Cu_2O formation in air oxidation [Figure 3.10]. A similar kind of temperature shift during oxidation of Cu films under various oxygen partial pressures has also been noticed [54]. It is quite clear that the formation of crystalline Cu_2O phase occurs for 140°C -240°C, whereas the CuO phase starts to appear only above 250°C, during annealing under oxygen ambient condition. A similar kind of phase transition from $Cu \rightarrow Cu_2O \rightarrow CuO$ during thermal oxidation of Cu films under an air ambient condition has already been observed [4, 50]. However, these oxidation temperatures are significantly lower from our earlier observation which can be explained in terms of oxygen partial pressure as it may significantly enhance by chemical reactivity of the copper atoms with the oxygen molecules as well as the oxygen diffusion process through the copper layer.

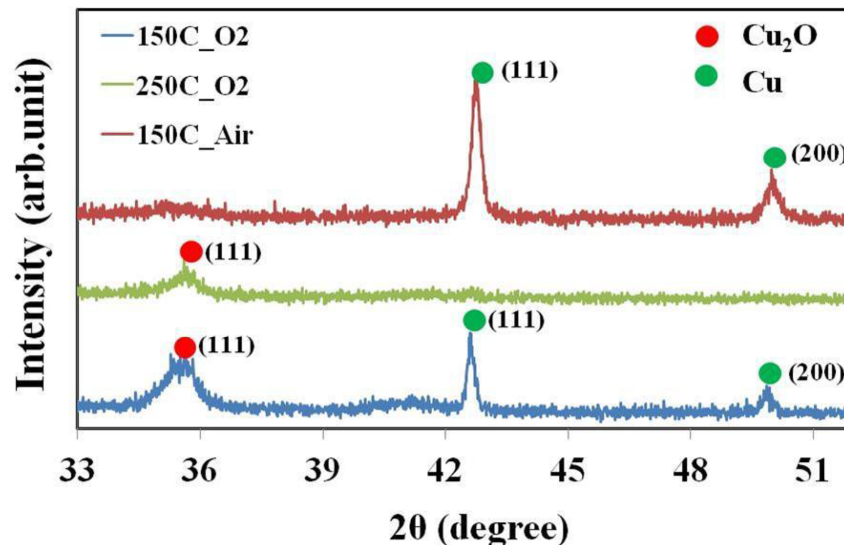

Figure 3.11: *XRD patterns of Cu layers oxidized at oxygen ambient at various temperatures and durations.*

3.3.1.6 Effect of crystallographic orientations

It can be noticed from our XRD results of Figure 3.7 and Figure 3.8 that the oxidation process of the Cu films may also be influenced by the crystallographic orientations of the

film surface. Although the glass substrate used for Cu deposition is amorphous and the deposited Cu films are of polycrystalline nature, a clear preferential growth of Cu grains along (111) lattice pale can clearly be observed from the earlier XRD results. Figure 3.7(a) and (b) represent the evolution of Cu_2O phase with the oxidation time. Initially, the (111) diffraction peak of Cu_2O starts to appear along with the Cu (111) and (200) diffraction lines. A clear growth preference of the (111) plane of Cu_2O over all other growth orientations is found. However, at the later stage towards the completion of the Cu_2O formation, (200) growth plane starts to dominate over the (111) growth plane of Cu_2O. On the other hand, no such preferential orientation is observed for the CuO growth. Figure 3.8(a) and (b) show both (-111) and (111) diffraction peaks start to appear from the beginning and maintain a relatively similar intensity profile throughout the formation of the CuO layer. These findings can be related to the initial crystalline orientation of the Cu grains where a dominating (111) plane is observed along with a weak (200) reflection. In addition, Cu and Cu_2O both exhibit a cubic crystal structure. The evolution of (200) diffraction peak at the later stage of Cu_2O formation may also be related to the relaxation of lattice stress of the oxide film through the rotational mismatch of the crystalline grains. Hence, a relatively faster oxidation may be expected at this stage due to the formation of additional grain boundaries [4, 33]. A faceted structure of (111) Cu_2O surface is also observed in STM imaging which will be discussed later.

3.3.1.7 Surface oxidation mechanism

For a better understanding of the thermal oxidation process of thin Cu film, a proposed schematic of surface oxidation is discussed in Figure 3.12. Native oxidation starts immediately after exposing the thin Cu films to the air ambient as represented in Figure 3.12(I a). In general, surrounding oxygen atoms are chemically adsorbed on the surface of almost all metals and form an invisible oxide layer (native oxide) [39].This layer usually acts as a diffusion barrier for O_2 and protects the film from further oxidation [Figure 3.12 (I a)]. For Cu film, thermal energy at 150°C overcomes the diffusion barrier and Cu_2O nucleation starts and expands laterally. Initial nucleation sites could be originated from any structural defects such as grain boundaries, dislocations, impurities etc. These clusters grow rapidly to form a Cu_2O film on Cu surface [Figure 3.12 (I c)]. Annealing accelerates the growth process of this protective film and

the oxidation reaction is controlled thermally. Assume that Cu-ions are more mobile in the oxide than the O-ions it diffuses outwards from the substrate to the interface which incorporate into the oxide network. Thus, oxide layers are formed at the interface and Cu_2O thickness increases [Figure 3.11, (II)]. For instance, the coexistence of Cu_2O and Cu phases has been detected below 320°C temperature.

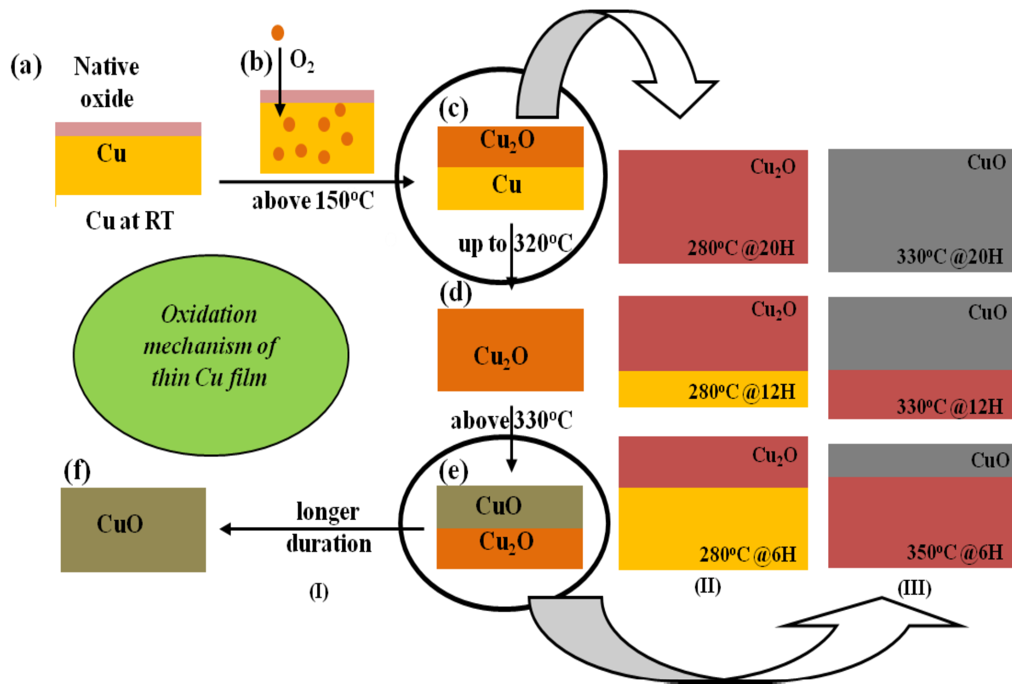

Figure 3.12: *Schematic representation of surface oxidation mechanism of thin copper films.*

However, the diffusion length increases with annealing temperature and duration and Cu converted completely into Cu_2O phase [Figure 3.12(I, d)]. However, activation energy of CuO formation demands a higher thermal energy (325 °C). Since, there is no more Cu left to be oxidize transformation of Cu_2O to CuO [Figure 3.12 (I, e-f) & (III)] starts to form above 330°C [32-33].However, in all cases, a longer duration of oxidation results in a thicker oxide layer whereas the oxidation temperature determines the oxide phase.

3.3.2 Properties of Copper Oxide thin films

Apart from the oxidation studies, different characterization techniques are also used for in depth studies of various analytical properties such as surface morphology, structural, electrical and optical properties as well as chemical composition of the thin copper oxide

films. These techniques are based on number of methods including X-ray photoelectron spectroscopy(XPS), energy dispersive X-ray spectroscopy(EDX), scanning electron microscope (SEM), atomic force microscopy (AFM), scanning tunneling microscopy (STM), transmission electron microscope (TEM), UV-Visible spectroscopy, Raman spectroscopy and four-point probe technique. The working and related theory of these characterization techniques are briefly described in Chapter 2.

3.3.2.1 Surface morphology of thin Cu oxide films

Surface morphology is an advanced form of high spatial resolution imaging, which is useful to produce sophisticated microscopy images of sample surfaces. In this aspect, FESEM is mostly used along with some AFM and STM imaging.

Scanning electron microscopy (FESEM)

The surface morphology of the copper oxide films, oxidized at different temperatures were analyzed with a commercial field emission scanning electron microscopy (FESEM) from Nova NanoSem 450, operated from 0.5 to 30 kV. It is found that the surface morphology of any film can very much depend on its growth parameters and the choice of the substrate. However, the surface morphology of the oxide films can highly be influenced by its materialistic property (oxidation state) rather than the growth mechanism (temperature, film thickness, duration) [4, 32, 38]. Figure 3.13 shows field emission scanning electron microscope (FESEM) images of 400 nm thin Cu films oxidized at different temperatures for 4 hours. The as-grown Cu film surface shows a smooth morphology and appears with uniformly distributed homogeneous clusters of 60-80 nm lateral size [Figure 3.13(a)].

However, the Cu_2O film surface appears with a very different surface morphology with highly faceted structures consisting of tetrahedron shaped islands which can clearly be seen after oxidation at 300°C [Figure 3.13(b)]. This faceted morphology is very much related to the structural characteristic of the cuprous oxide [4, 33, 40]. Figure 3.13(c) depicts the surface morphology of a CuO film oxidized at 350°C for 3 hours. A relatively rough surface morphology with in homogeneously grown granular layered structures is found after oxidation in air at 350°C. Transition of the faceted Cu_2O structures into a rough granular surface morphology may be

related to the transition of cubic Cu_2O to monoclinic CuO layer. A homogeneous and faceted surface morphology of CuO film has been observed after a longer oxidation for 9 hr [Figure 3.13(d)].

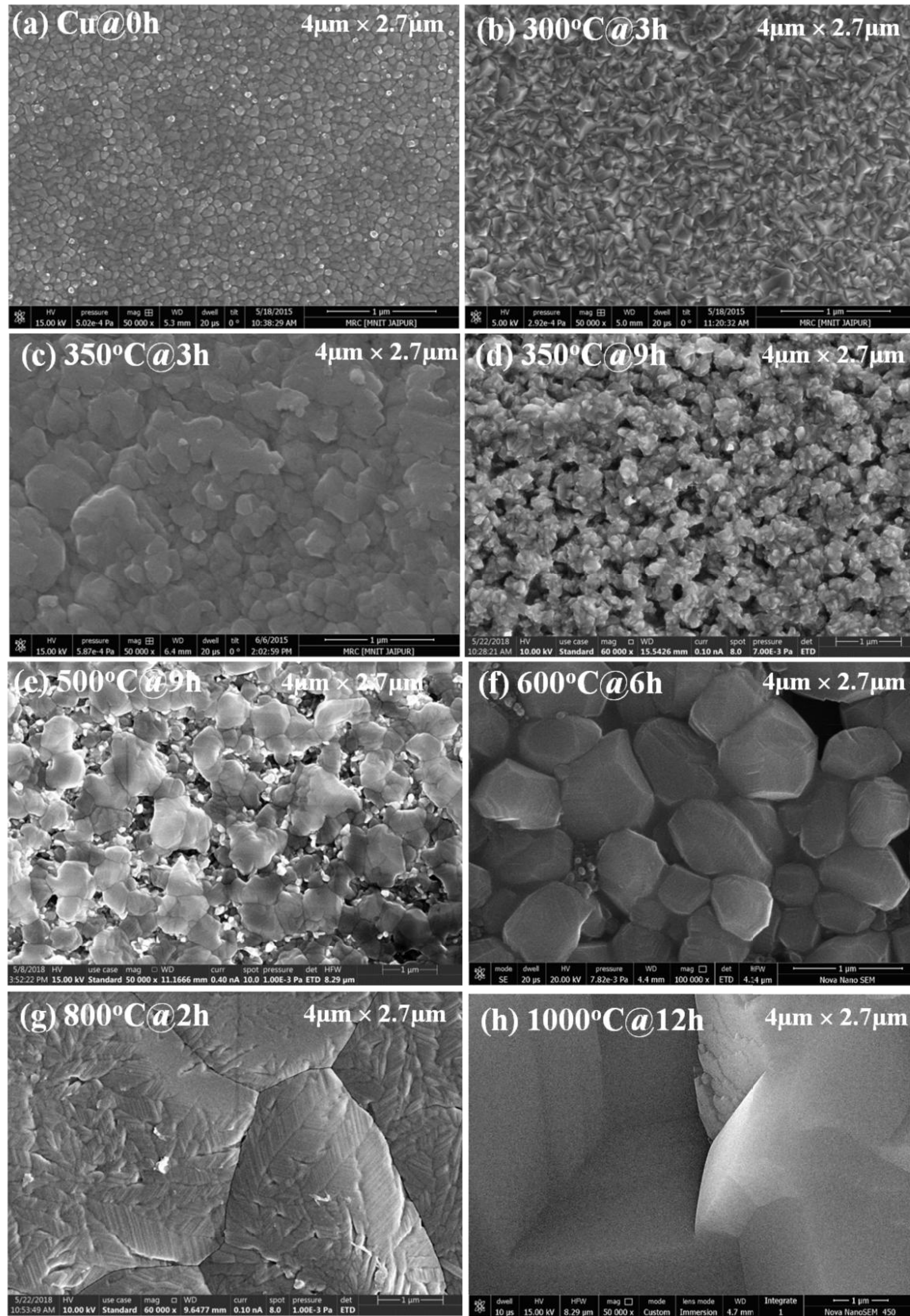

Figure 3.13: *SEM image of 400 nm thick Cu films on glass substrate: (a) as-grown (b) oxidized at 300°C, (c) 350°C for 3hrs annealing and (d) 350°C for 9hrs, (e) 500°C for 9hrs, (f) 600°C for 6hrs, (g)800°C for 2 hrs and (h)1000°C for 2hrs, respectively.*

However, oxidation at even higher temperature results in faceted CuO nanostructures with larger crystallite size [Figure 3.13(e-h)]. Higher thermal mobility results in an improved crystalline phase as well as the coalescence of the smaller grains into a larger grain [4, 33]. However, annealing at even higher temperatures (500°C - 1000°C), results in a CuO nanostructures with larger crystallite grains as represents in Figure 3.13(e-h). This is mainly due to the increased surface energy and large diffusion length at higher oxidation temperature [50]. Formation of larger grains at higher temperature is due to the thermal mobility and stronger diffusion of oxide materials and transfer of atoms across the grain boundary which finally leads to coalescence of smaller grain into a larger one [4, 32-33].

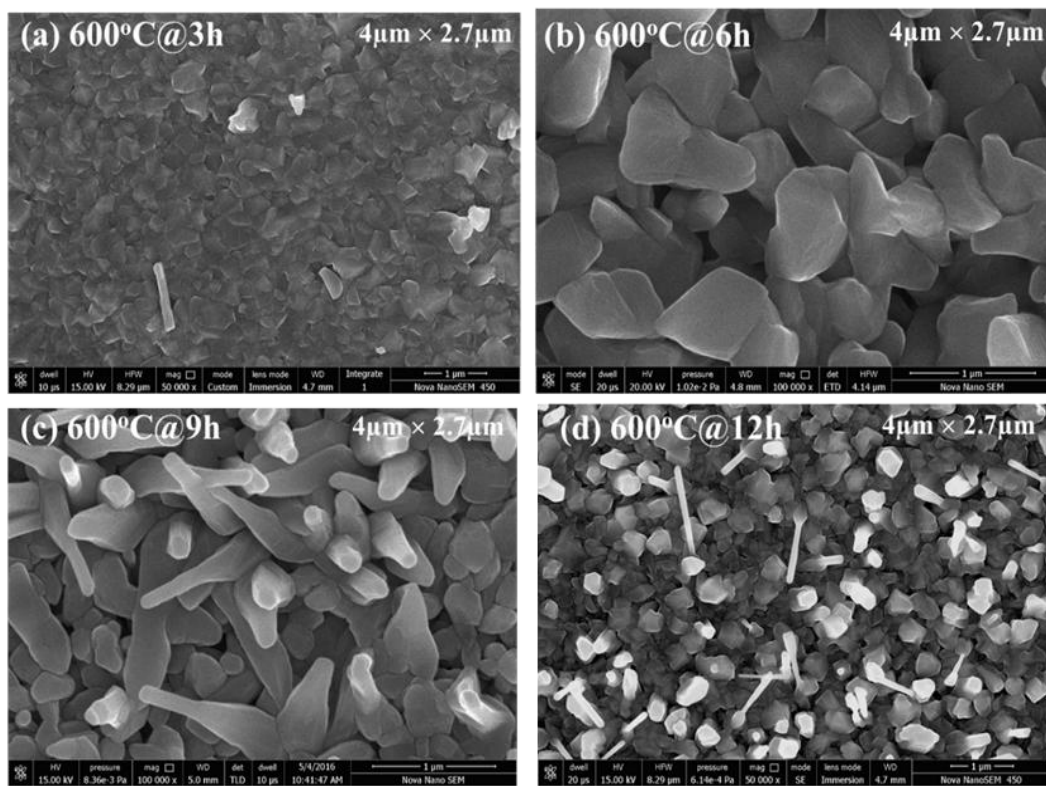

Figure 3.14: *SEM image of 400 nm thick Cu films oxidized at 600°C for different duration of annealing (a) 3hrs, (b) 6hrs, (c) 9hrs and (e) 12hrson glass substrate.*

In addition to thermal diffusion, duration of oxidation can also significantly influence on the surface morphology of CuO film, by systematically controlling the surface kinetics. Figure 3.14 [(a)-(d)] demonstrates the surface morphology of thin CuO films formed at 600°C oxidation temperature for different annealing durations (3-12 hrs). Apart from an increase in grain size, a strong asymmetric growth towards the formation

of CuO nano-rods has clearly been observed while increasing the annealing duration from 3hrs $\rightarrow$ 12 hrs. CuO nano-rods are having a uniform length of 500nm to 2.5μm and exhibited a high degree of vertical alignment. However, a small fraction of inclined growth is also found in CuO thin films [4, 33]. Formation of larger grain size can be explained by longer diffusion kinetics, keeping the diffusion process within the thermodynamic limit. The asymmetric growth leading towards nano-rods formation is mostly driven by the lowering the surface energy of the CuO nano-rods at this growth temperature. However, a very small oxidation temperature window is available for the formation of single phase of Cu_2O thin films. Hence, it is very difficult to find any temperature dependent significant morphological changes for Cu_2O thin films.

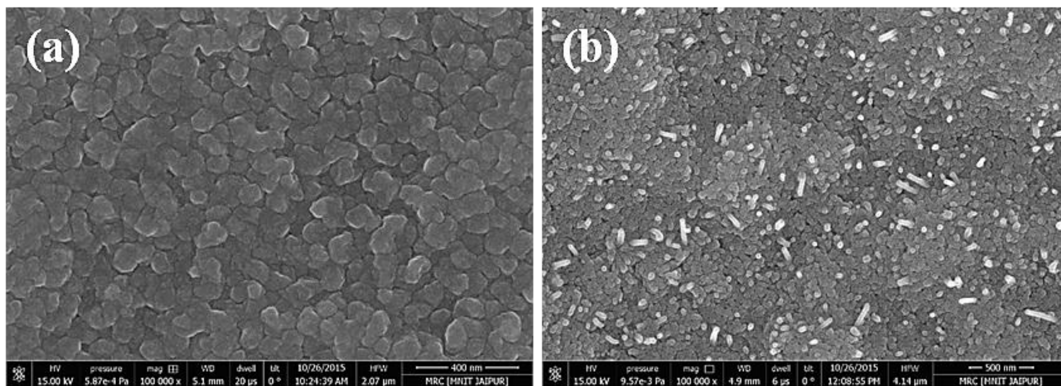

Figure 3.15: *FESEM images of thermally oxygenized Cu films in oxygen ambient at (a) 200^oC for 3 hours for single Cu_2O phase, (b) 300^oC for 3 hours for single CuO phase.*

The morphological evolution of thin Cu_2O and CuO films during oxidation under oxygen ambient annealing condition is shown in Figure 3.15. After oxidation of Cu films at 200^oC for 3 hours, single phase Cu_2O films are formed which appear in a granular island structure as shown in Figure 3.15 (a) [38, 41]. Whereas, annealing at 300^oC for 3 hours results in a strong growth asymmetry with formation of CuO nano-rods, as can be seen in Figure 3.15(b). In contrast to faceted surface morphology of Cu_2O surface during air annealing at 300^oC [Figure 3.13(b)], granular morphology of Cu_2O surface can be related to a lower surface energy and diffusion kinetics at a lower oxidation temperature of 200^oC. However, for asymmetric CuO nano-rods growth during O_2 ambient oxidation at 300^oC can be explained in this way. The lower surface diffusion at a lower temperature can be compensated here by a higher O_2 concentration. As a result,

CuO nano-rods grow at 300°C during O_2 ambient oxidation. A similar kind of CuO nano-wires formation has also been reported by *L.S. Huang et al.* during thermal oxidation ofthin Cu foil in oxygen ambient condition [41].

Atomic force microscopy (AFM)

The surface topography and roughness of copper oxide films have been characterized using a commercial atomic force microscope. Figure 3.16 presents the 3D AFM images (10μm × 10μm) of the as deposited Cu film as well as oxidized in air at temperature of 300°C [Cu_2O Figure 3.16(b)] and 350°C [CuO Figure 3.16(c)] for 3hrs. The surface topography of copper oxide thin films confirms that the grains are uniformly distributed, compact and have good adherence to the glass substrate. The surface of as-grown copper film [Figure 3.16(a)] is quite smooth with uniform and homogeneous grain having a roughness (rms) of less than 1 nm. These uniform grains are heavily packed and form a smooth surface texture. In Figure 3.16(b), the surface morphology of Cu_2O film reveals that the surface roughness increases significantly which is also complementary with the faceted surface morphology of Cu_2O surface observed in SEM imaging. High surface transport during the oxidation process (material phase change) results in a rougher surface morphology [Figure 3.16(b)]. With increase in annealing temperature, oxide nucleates are now combined together to form a continuous Cu_2O film.

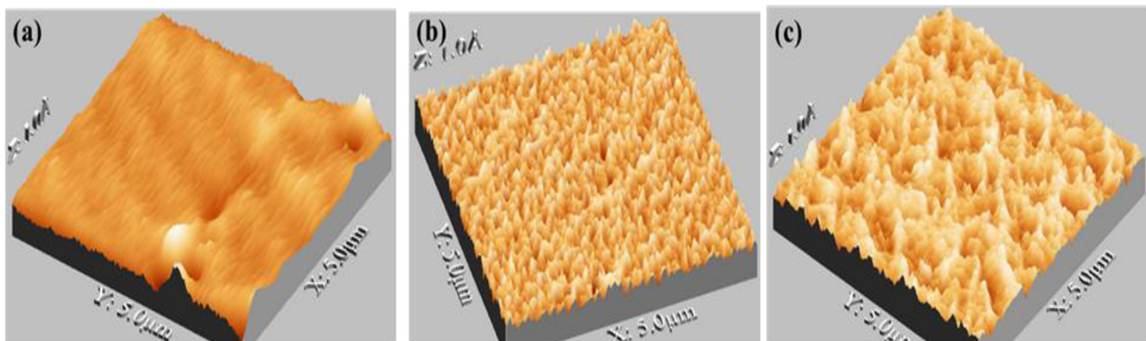

Figure 3.16: *AFM image of thin Cu films on glass substrate: (a) as-grown (b) oxidized at 300°C and (c) 350°C, respectively, in air ambient.*

A similar trend is also followed during the transition/formation of the Cu_2O film to CuO. A result, surface texture gets further rougher as shown in Figure 3.16(c)

The AFM results also reveal that the size of the CuO grains increases with oxidation temperature from 350 to 500°C when the surface roughness also decreases. This behavior can be attributed to the random distributions of the smaller grains at lower temperature which turns to larger one and hence lower the surface roughness [42-43].

Scanning tunnelling microscopy (STM)

To investigate the surface topography of the faceted Cu_2O films in details and with a higher surface resolution, ultra-high vacuum (UHV) scanning tunneling microscopy (STM) from Omicron Nanotechnology GmbH has been used as a characterization tool. Before any STM imaging, samples were out gassed at 100°C for 2 hr under an UHV condition to remove any kind of physi-absorbed contaminations during the exposure in air. Scanning was performed in a constant current mode with a tip bias of 2V and tunneling current of 50 pA. The surface morphology appears to be quite rough in STM imaging. However, many triangular island with flat top surface have been observed as shown in Figure 3.17.

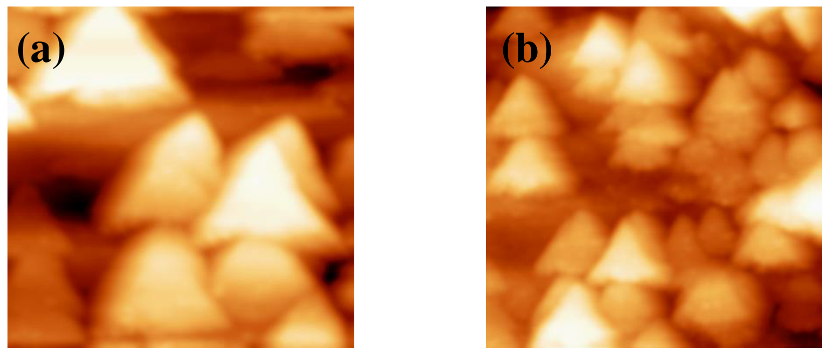

Figure 3.17: *STM images of thin Cu_2O films on glass substrate showing flat islands of triangular shape grown at 300°C. Scan areas (a) 500 nm × 500 nm and (b) 250 nm × 250 nm.*

Moreover, these triangular island are having a clear preferential orientation with three-fold symmetry. We assume this triangular top facet is related to (111) crystal plane of Cu_2O which arises from a truncated cubic structure along its body diagonal. Although there is no direct evidence of (111) crystal plane, but a strong XRD peak for (111) reflection suggest it preference. Apart from morphological studies suing STM scanning tunneling spectroscopy (STS) was also employed to find the local surface electronic

property down to nanometer scale. A clear difference in raster spectroscopy suggests that the electronic properties of the island surface are distinctly different from other surface area [Figure 3.18].

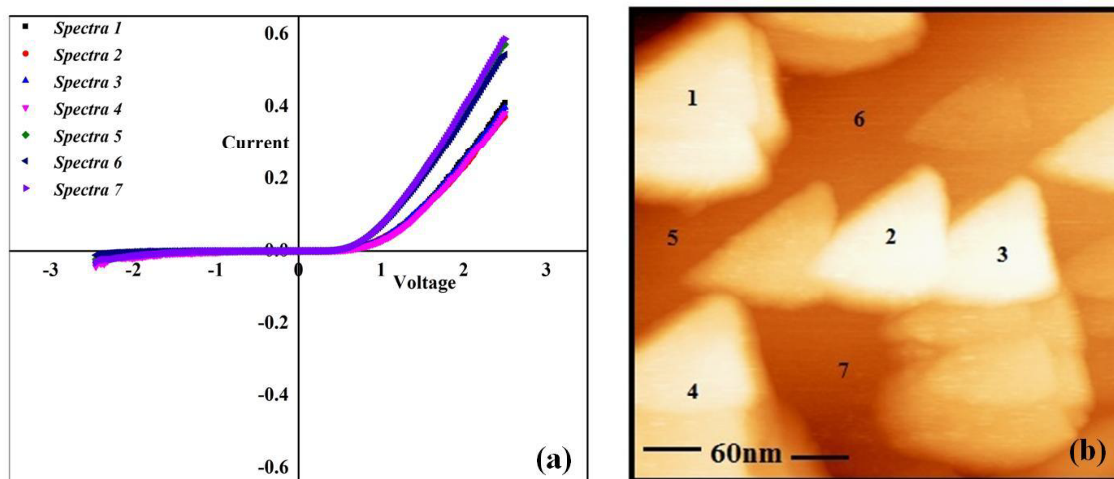

Figure 3.18: *Raster spectroscopy of thin Cu_2O films showing flat islands of triangular shape are electronically different from the other surface parts of the STM image. Scan areas (a) 300nm × 300 nm.*

3.3.2.2 Optical properties of thin Cu oxide films

Various optical properties of thin copper oxide films have been studied using UV-visible spectroscopy and Raman spectroscopy. In general, Raman spectroscopy is used to study the inelastic scattering of photon with the material which further gives the chemical information. This method is employed here to study the composition or oxide phase of the Cu films. UV-visible spectroscopy is used for the investigation of the optical properties such as transmission, absorption, reflection, refraction, polarization and interference. Here we use this technique to calculate the optical band gap (direct and indirect) of the copper oxide materials.

Raman spectroscopy

Raman spectroscopy measurements have been carried out using a commercial Raman unit from Horiba Scientific to identify the various oxide phases of the copper film. The room

temperature Raman spectroscopy measurements of the thin oxide films are performed within the spectral region of 50-900cm^{-1}. Figure 3.19(a) represents the micro-Raman spectroscopy of thin Cu, Cu_2O (annealed at 300°C for 3h), mixed oxide (Cu_2O + CuO) and CuO (annealed at 350°C for 3h) films. A typical Raman spectrum obtained from nano-crystalline Cu_2O thin films exhibits two strong peaks at 217 cm^{-1} and 146 cm^{-1}, correspond to the Cu_2O oxide phase [31, 33]. In case of CuO, three peaks centered at 292, 341 and 626 cm^{-1} are observed, which can be identified as the first order A_g and $2B_g$ phonon scattering [33, 42]. For thin films of mixed oxide phases Raman spectra show a combination of both set of peaks assigned to Cu_2O and CuO. In general, the Raman spectroscopy results are in good agreement with our XRD findings and reveal a similar kind of phase transformation of the Cu_2O to CuO during oxidation at a temperature above 320°C. However, oxidation of the Cu films at a lower temperature, between 150°C to 250°C, Raman data reveals very different information in contrast to our earlier XRD findings. A clear existence of Raman peaks at 146 cm^{-1} and 217 cm^{-1} is observed after oxidation of a Cu film at 220°C for 4 hours, which clearly indicates the presence of Cu_2O phase [Figure 3.19 (b)].

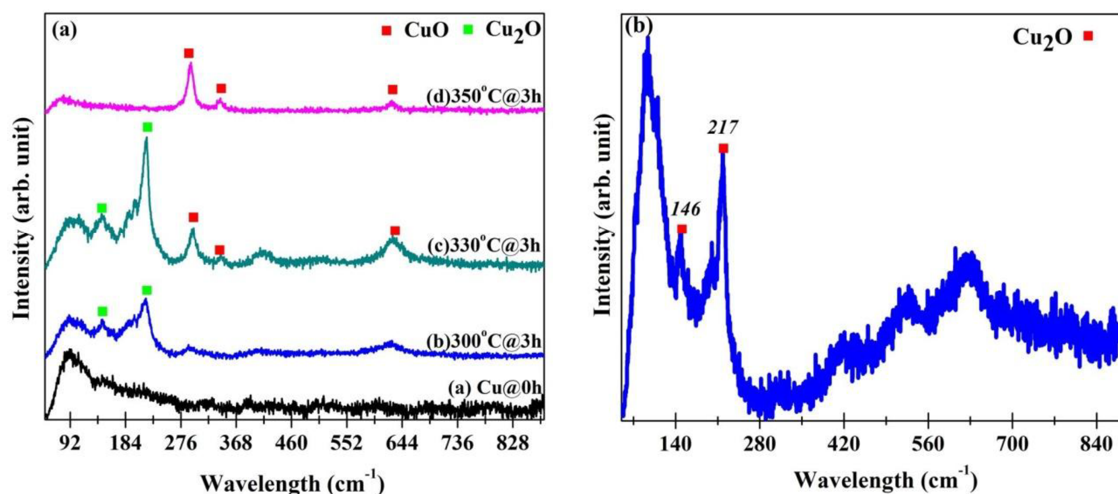

Figure 3.19: *Raman spectra of various Cu oxides films grown by thermal oxidation of thin Cu films in air. Inset shows the Raman spectrum of Cu film oxidized at 220°C for 4 hours in air.*

Whereas, XRD result does not show any trace of Cu_2O (111) reflection peak and appears only with the Cu diffraction lines. Thus, based on the Raman and the XRD analysis, it can be concluded that both Cu and Cu_2O phases coexist within the oxidized films. This finding is also consistent with our four probe resistivity measurement where the oxide formation of

the Cu film is predicted above 150°C. XRD analysis could not detect the presence of Cu_2O due to the following reason. As a fact, XRD can only detect crystalline grains of sufficient size of the oxide material, whereas Raman technique is capable of detecting the amorphous states too. In addition, Raman spectroscopy is much more surface sensitive as compared to the XRD. Since the Cu_2O phase starts to form through surface oxidation, it would be easier with Raman spectroscopy to detect even for a very thin over-layer of oxide on Cu film rather than the XRD can detect only after a significant amount of surface oxidation. A similar kind of discrepancy has also been reported by other researchers [33].

Therefore, the uncertainty can be solved in the following manner: Oxidation of the Cu films below 250°C results in a mixed phase of Cu and Cu_2O. Either the oxide layer is very thin or all the grains are very small (poor crystalline state). These assumptions are well justified by a very limited thermal diffusion of oxidizing species and Cu atoms at lower oxidation temperature. As discussed earlier, native oxide layer acts here as a diffusion barrier and with increase in annealing temperature diffusion above 150°C, thermal energy starts to overcome the barrier and oxidation continues. However, the diffusion process at this temperature still remains very much limited which may result in a poor crystalline state of the Cu_2O layer. As the ambiguity of the 4-probe resistivity and the XRD measurements is solved, for a better understanding of thermal oxidation mechanism, we introduce a schematic of the surface oxidation process of thin copper films already discussed in subsection 3.1.7 [Figure 3.12]. Exposure of a fresh copper film to air ambient results in a spontaneous native oxide formation, which later acts as a diffusion barrier for O_2 and prevents the further oxidation. The thermal energy at 150°C, overcomes the diffusion barrier and Cu_2O formation starts. However, activation energy of CuO formation demands a higher thermal energy (325°C) [33].

UV-visible spectroscopy

To identify the oxide phase of the Cu thin films grown at elevated temperature, optical band gap of the oxide films are estimated using a Simazu UV-visible optical spectroscopy. Optical transmittance of the oxide films was recorded within the wavelength range of 300-800 cm^{-1}. Figure 3.20 (a) shows the optical transmission spectra of CuO_x thin films of different thicknesses.

In addition, the absorption coefficient (α) is also plotted against the photon energy *(E_g)* to estimate the optical band gap of thin Cu_2O films. The absorption coefficient (α) is determined with the help of "Kubelka - Munk formula" is $F(R) = (1-R)^2/ 2R$. Where, R is the reflectance, and F(R) is proportional to the absorption coefficient (α) [43].

The photon energy is calculated by using *hc/λ*, where h represents the Planck's constant and λ is the wavelength in nm. Finally, the optical band gap is estimated by linear extrapolation, as can be seen in Figure 3.20 (b). The result shows a direct band gap of nearly 2.1 - 2.3 eV, which lies well within the visible light range and also suggests a single oxide phase of Cu_2O thin film is formed [4, 33, 36]. Whereas, the optical band gap of the CuO thin film grown at 450°C is also shows a direct band gap of about 1.5 eV which suggests a single CuO phase is observed [Figure 3.20 (c & d)] [45-46].

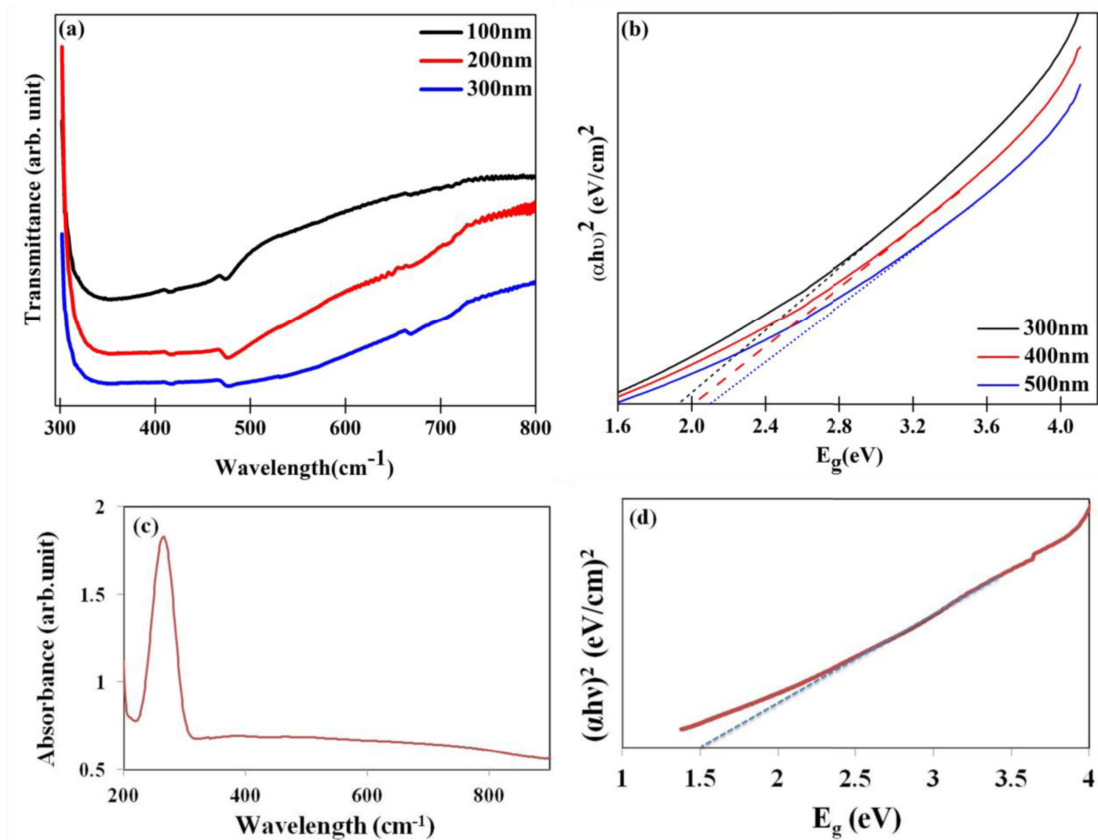

Figure 3.20: *UV-visible spectra of (a) Cu_2O and (b) CuO thin films grown by thermal oxidation in air ambient. Inset shows the optical band gap for different CuOx thin film thicknesses.*

3.3.2.3 Chemical properties of thin Cu oxide films

For further investigation about the chemical purity of the copper oxide phase with a very high sensitivity, X-ray photoelectron spectroscopy (XPS) and Energy Dispersive X-ray (EDX) analysis techniques were employed here. XPS technique is extremely surface sensitive and provides a quantitative analysis about surface chemistry whereas EDS gives nice complementary information between SEM morphology and qualitative information surface chemistry.

X-ray photoemission spectroscopy (XPS)

X-ray photoemission spectroscopy (XPS) measurement was performed to find the oxidation states of Cu and the oxide phase purity with an extremely sensitive manner. During XPS measurements, the base pressure of the chamber was maintained below $<10^{-9}$ mBar and monochromatic Al K_{α} (1486.6 eV) and Mg K_{α} (1256.7 eV) lines were used as X-ray sources. All binding energies of the emitted photoelectrons are calibrated to the C1s line positioned at 284.5 eV of the contaminant from the ambient. Figure 3.21(a) shows wide scan XPS spectra of thin Cu films of metallic and their oxides phases. The survey scans appear with the copper core level peaks of Cu2p (951.5 eV and 932.6 eV), Cu3s (120.6 eV) and Cu3p (75.9 eV) and Cu LMM Auger peaks ($L_3M_{45}M_{45}$ at 568 eV, $L_3M_{23}M_{45}$ at 638 eV and $L_3M_{23}M_{23}$ at 715 eV), along with additional peaks of C1s (285 eV) and O1s (530.1 eV). Figures 3.20 (b) & (c) present high resolution scans of Cu2p core level spectra and LMM Auger transmission lines, respectively. Three different chemical states of the Cu films (Cu, Cu_2O and CuO) are clearly marked and the relative shifts in peak positions of the binding energies are compared.

Figure 3.21(b) shows high resolution Cu2p XPS data recorded for the copper thin film oxidized at 300°C and 350°C for 3 hours. It can be seen that Cu2p energy level of Cu and Cu_2O are composed of main characteristic doublet peaks correspond to $Cu2p_{1/2}$ and $Cu2p_{3/2}$, respectively, with a spin-orbit splitting of 19 eV. This is in good agreement with the values reported in the literature [42, 46-47]. However, in case of CuO film, additional shake-up satellite peaks at 8 eV higher binding energy of the main Cu2p peak, originate from multiple excitations in copper oxides, are also found. These

satellite peaks are known to be the characteristics of CuO phase [42, 33]. $Cu2p_{3/2}$ binding energy peak of Cu^{+} oxidation state of Cu_2O film appears at 932.65 eV which is very close to the metallic Cu^{0} state of Cu film centered at 932.4 eV. However, a significant shift of about 1 eV towards higher BE side (933.65 eV) is found for Cu^{+2} oxidation state of CuO film. Well defined shake-up satellite peaks associated with the $Cu2p_{3/2}$ line also appeared. As there are no significant differences in the $Cu2p_{3/2}$ BE spectra for Cu and Cu_2O, it is difficult to determine the metallic Cu^{0} phase within the Cu_2O oxide phase for Cu2p scan.

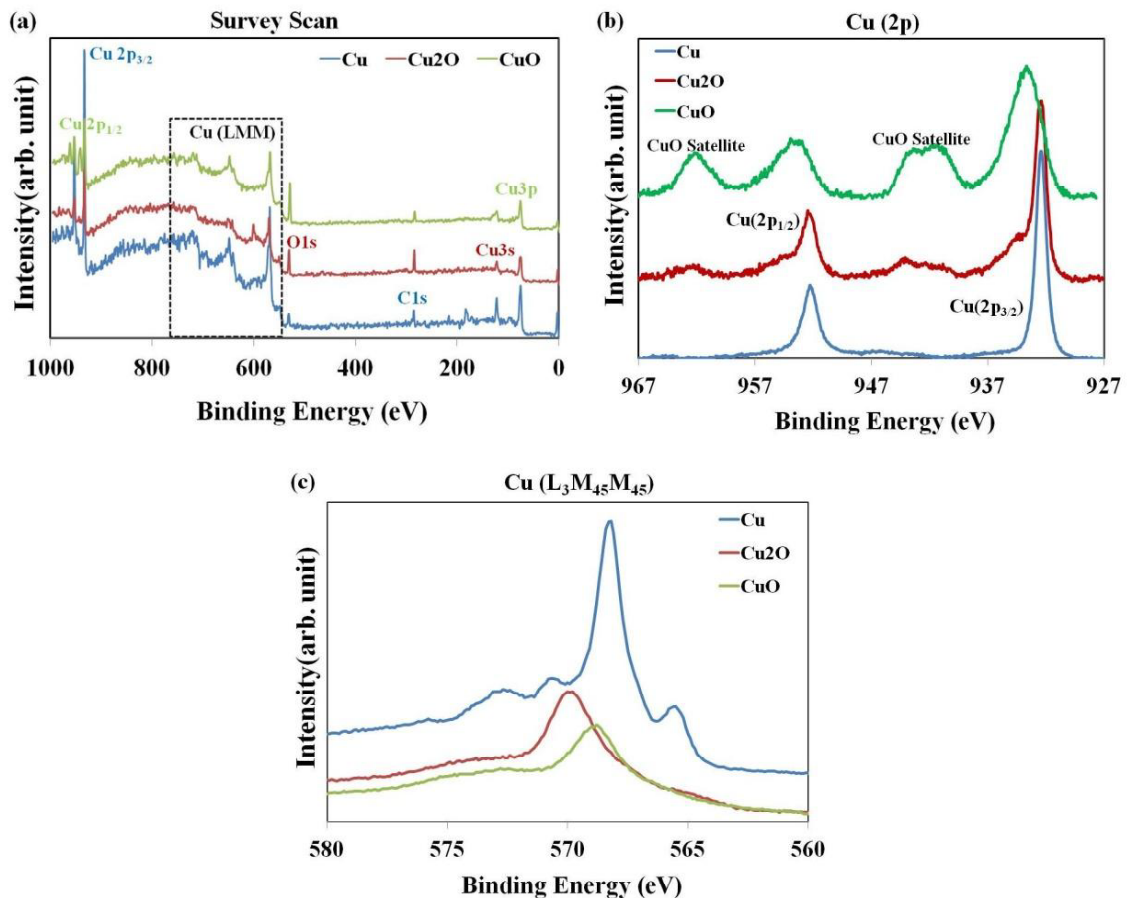

Figure 3.21: *XPS spectra of different Cu oxide films: (a) Wide Scan (b) Cu2p core level and (c) LMM Auger spectra.*

To eliminate this possibility, we compare the Auger $L_3M_{45}M_{45}$ spectra of these films where a clear separation in the peak positions for metallic Cu (567.8 eV), Cu_2O (570.15 eV) and CuO (568.5 eV) has been noticed as shown in Figure 3.21(c) [62-63]. In XPS measurements the probing depth within the Cu oxide layer is expected to be only ~2 nm for incident photon energy of 1486.6 eV (Al Kαline) [33, 42, 48]. This makes XPS

highly surface sensitive. Even, the satellite peaks corresponding to the Cu^{+2} oxidation state are not observed for Cu_2O film surface, which confirms the phase purity of the film. Therefore, from all above findings (XRD, Raman spectroscopy and XPS) it can be concluded that within a particular range of oxidation temperature, a single oxide phase of crystalline Cu_2O film can be formed by thermal oxidation in an air ambient.

For further investigation about the quantitative analysis and oxidation states of CuO thin films, XPS measurement has been examined using two different samples [Figure 3.22]. In addition, a relative comparison of oxidation temperature dependent surface chemical stoichiometry is also calculated here. Figure 3.22 (a) shows wide scan XPS spectra of three different CuO films grown at 330°C, 400 and 600°C, respectively. In general all, all survey scans look similar and appear with the different copper core level [Cu2p (951.5 eV and 932.6 eV), Cu3s (120.6 eV) and Cu3p (75.9 eV)] and LMM Auger [$L_3M_{45}M_{45}$ (336 eV), $L_3M_{23}M_{45}$ (412) eV and $L_3M_{23}M_{23}$ (485 eV)] binding energy (BE) peaks, along with O1s (530 eV) and C1s (284.5 eV). Well defined shake-up satellite peaks of Cu2p lines for CuO oxide phase, characteristic of Cu^{+2} oxidation state, are also observed towards the higher BE [10, 5, 49]. To find the minor chemical changes in CuO samples due to their oxidation temperature, a comparative study between 330°C and 600°C CuO films are performed for O1s and $Cu2p_{3/2}$ BE peaks. Figures 3.22 (b) & (c) represent high resolution scans of O1s and $Cu2p_{3/2}$ BE spectra, respectively, for CuO film grown at 330°C. Whereas, Figure 3.22 (d) & (e) represent the same for CuO film grown at 600°C. Different chemical states of O and Cu atoms are clearly marked and a relative comparison of BE peak intensities are compared. Figure 3.22 (b) and (d) show high resolution O1s XPS data recorded for CuO films oxidized at 330 °C and 600 °C, respectively. It can clearly be seen that O1s spectra are composed of two peaks. Sharp peaks towards lower BE (530 eV) is originated from the O^{-2} state within the CuO crystal whereas relatively broader peaks with 1 eV higher BE (531 eV) is attributed to the adsorbed and defect states of oxygen on the CuO surface. Similarly, $Cu2p_{3/2}$ peaks correspond to different oxidation states of Cu are depicted in Figure 3.22 (c) and (e). The de-convoluted spectra appear with 4 peaks, originated mainly from Cu^{+2} (933.7 eV) and shake-up satellite states [S1 (941 eV) and S2 (943.5 eV)], along with a weak Cu^{+} state (932.6 eV). For better understanding and clarity, every detail of all of de-convoluted spectra is summarized in Table 3.3(a).

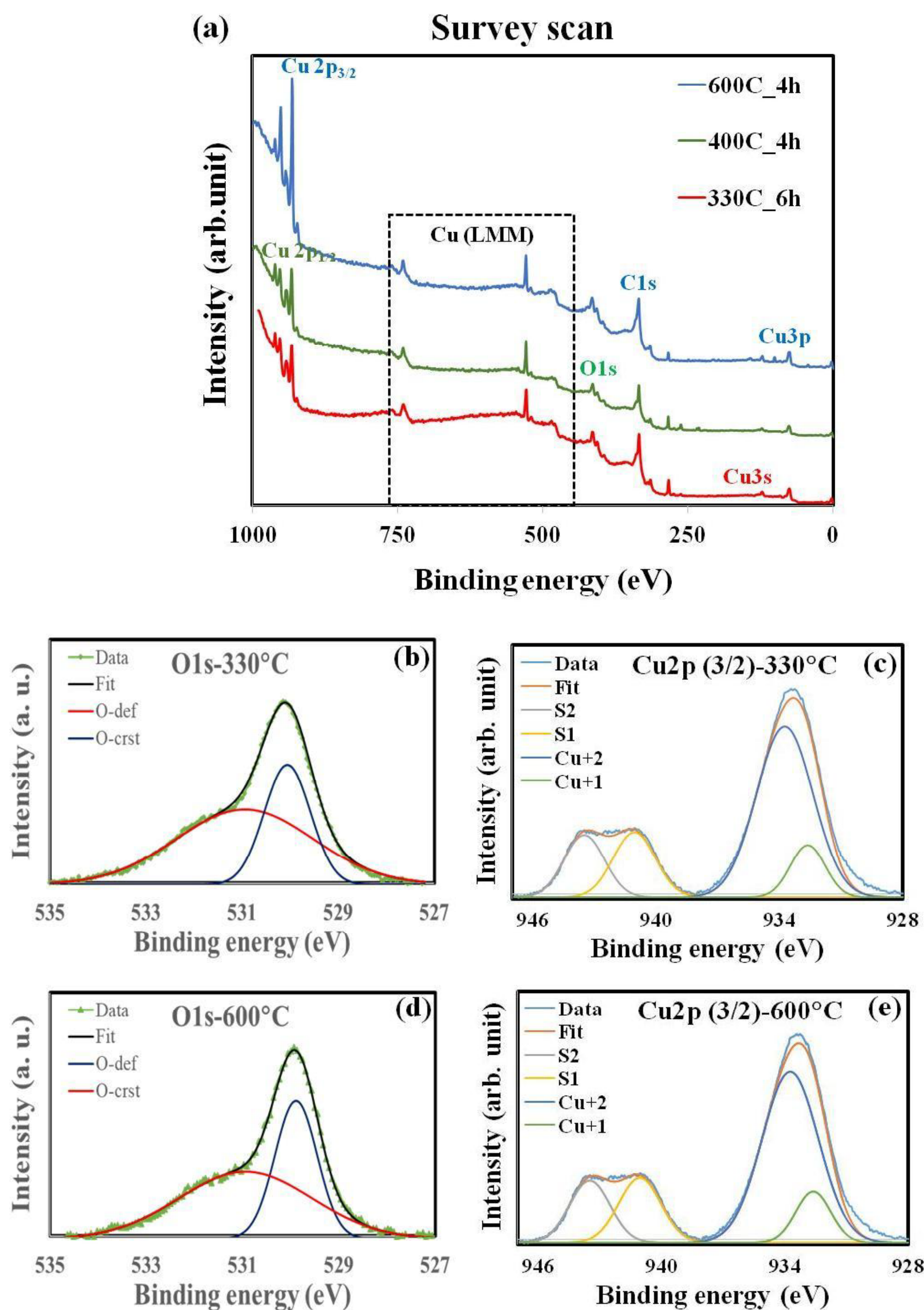

Figure 3.22: *XPS spectra of CuO films with different oxidation temperatures: (a) XPS survey Scan of 330℃, 400 and 600℃. High resolution scans for 330℃: (b) O1s and (c) $Cu2p_{3/2}$. High resolution scans for 600℃: (d) O1s and (e) $Cu2p_{3/2}$.*

Table 3.3: *(a) Binding energy positions and relative peak intensities of de-convoluted O1s and Cu2p$_{3/2}$ spectra of CuO thin films oxidized at 330℃ and 600℃, respectively.(b)Relative intensity ratio of O-crst vs Cu2p$_{3/2}$ (total), Cu^{+} vs Cu^{+} and O-crst vs O-def.*

Sample Name	BE Peak	Sub-peaks	Position	Area
CuO 330°C	O1s	O-def	531	38250
		O-crst	530	20696
	Cu2p$_{3/2}$	S2	943.5	34069
		S1	941.1	37048
		Cu^{+2}	933.7	130086
		Cu^{+}	932.6	24214
CuO 600°C	O1s	O-def	530.9	23763
		O-crst	529.9	15578
	Cu2p$_{3/2}$	S2	943.6	24823
		S1	941.2	18469
		Cu^{+2}	933.8	87700
		Cu^{+}	932.7	8638

Sample	Ratio 1		Ratio 2		Ratio 3	
	O-crst	Cu2p (total)	Cu^{+}	Cu^{+2}	O-crst	O-def
CuO-330°C	0.1341		0.1861		0.5411	
CuO-600°C	0.1617		0.0985		0.6556	

Although, both O1s and Cu2p$_{3/2}$ de-convoluted spectra appear quite similar but there are some significant quantitative differences which are summarize in Table 3.3 (b). Intensity ratio of oxygen species within CuO crystal (O-crst) to the total Cu2p$_{3/2}$ states (*i.e,* sum of all Cu^{+2}, Cu^{+}, S1 and S2) relatively increases from 0.13 for CuO film grown at 330°C to 0.16 for 600 °C grown film surface. This is a clear indication of enrichment of oxygen content within the CuO film grown at 600°C. Similarly, a convincing increase in Cu^{+2} state with respect to the Cu^{+} state can also be seen [Figure 3.22(c) & (e)]. The ratio of Cu^{+} to Cu^{+2} states is found to be decreased from 0.19 (CuO-330°C) to 0.1 (CuO-600°C), which further suggests a relative increase of 'CuO' oxide phase and hence the O_2 content within the CuO film [50]. In addition, the ratio of O-crst to O-def states is

also calculated and compared for both samples. An increase from 0.54 to 0.66 for CuO-330°C to CuO-600°C samples is also found. These findings are very much complementary with our earlier electrical characterizations and in good agreement with other reported works [51-52].

In the below, sub-section "Electrical characterizations', it is observed that the oxidation temperatures for CuO formation can significantly alter the surface resistivity of CuO due to a change in carrier concentration. From all XPS observations it is quite obvious that increase in oxidation temperature results in an enhanced O_2 species within the CuO film. CuO is by nature a p-type semiconductor which is explained with its Cu vacancy model. Hence, a relative increase in O_2 species within CuO will resultantly promote the Cu vacancy formation. Therefore, an enhanced carrier (hole) concentration for CuO is expected for higher oxidation temperature as found in Hall measurements studies. Finally, a decrease in surface resistivity for CuO film grown at higher oxidation temperature is also predicted which is also complementary with our earlier I-V results.

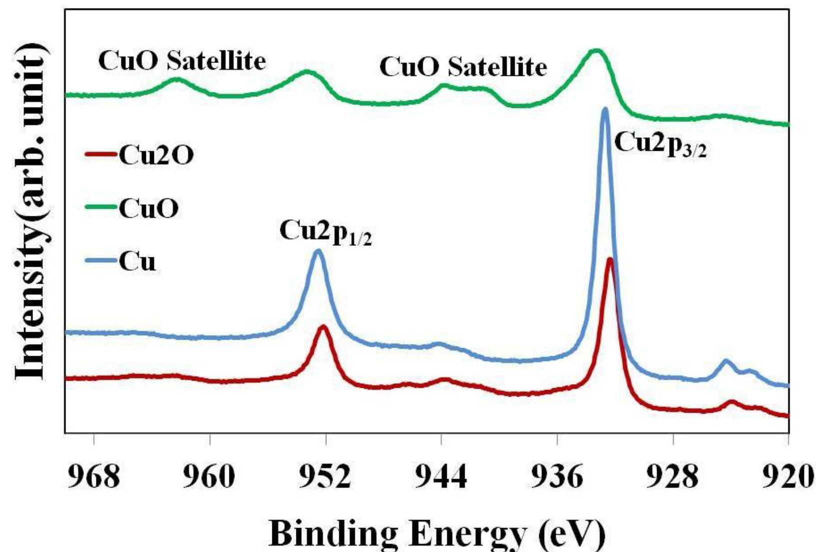

Figure 3.23: *XPS spectra of thermally oxidized thin Cu films in an oxygen ambient condition.*

As discussed in the XRD results of section 4.1 (oxidation process of copper oxide thin films) that the oxidation temperatures for Cu_2O and CuO phases can significantly differ in an air ambient with respect to an oxygen ambient conditions. The lowering value of the oxidation temperatures under oxygen ambient condition has also been confirmed from the XPS studies, as shown in Figure 3.23. In case of

oxidation at 250°C under oxygen ambient, XPS spectrum appears with the existence of a strong shake-up satellite peak of Cu2p, characteristic of the Cu^{+2} oxidation state of CuO. Moreover, oxidation of clean Cu films under low vacuum condition is also performed where the overall oxygen pressure was maintained much lower than the air ambient (<10^{-3} mbar).

A drastic shift of the oxidation temperature range towards higher value is expected here. Finally, it is also observed that the copper oxide films can completely be reduced to metallic copper by out gassing under an ultra-high vacuum condition (10^{-9} mbar) at an elevated temperature above 700°C. Therefore, from all these observations it is quite clear that the partial pressure of O_2 can significantly alter the final oxide phase of the Cu films. *Wong et. al* has also reported the effect of O_2 partial pressure towards the determination of the copper oxide phase during sputter growth process [53].

Energy dispersive Spectroscopy (EDS)

Chemical characterizations of copper oxide thin films along with their surface morphology are also conducted using the Energy Dispersive X-ray (EDX) analysis technique coupled with the FESEM system. EDX spectrum of copper oxide thin films, prepared at 300°C and 350°C in air ambient and 200°C and 300°C in oxygen ambient for 3hrs are shown in Figure 3.24(a-d), respectively. All EDX spectra obtained from Cu_2O and CuO thin reveal the clear presence of copper and oxygen peaks even with a weak silicon footstep from the glass substrate.

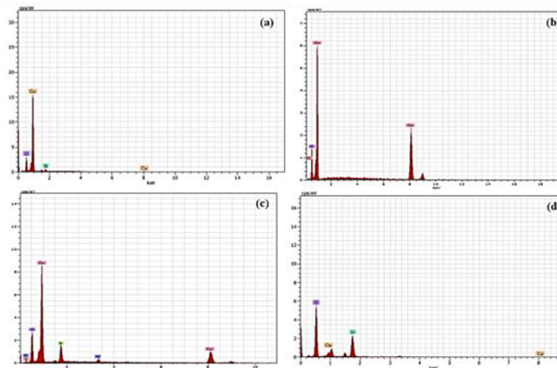

Figure 3.24: *EDX spectrum of copper oxide thin film, prepared by 3hrs of oxidation at (a) 300°C (b) 350°C in air ambient and (c) 200°C, (d) 300°C in oxygen ambient.*

Table 3.4: *EDX elemental analysis of samples oxidized for 3hrs at 300°C, 350°C in air and 200°C, 300°C in oxygen ambient.*

Sample Name	**Copper (%)**	**Oxygen (%)**
Cu_2O @ 300°C in air	87.91	10.79
CuO @ 350°C in air	61.73	15.82
Cu_2O @ 200°C in oxygen	57.23	22.57
CuO @ 300°C in oxygen	1.53	81.96

A summary of the EDX analysis is shown in Table 3.4, where the elemental compositions of Cu and O for Cu_2O and CuO films prepared in air oxygen ambient are shown. It has to be taken into account that EDS is not so sensitive for a quantitative analysis and the elemental compositions may drastically vary from place to place.

3.3.2.4 Electrical Characterization

Various electrical properties of the copper oxide thin films are characterized using four point probes technique includes sheet resistance/ surface resistivity as well as Hall Effect measurements. For resistivity measurements, contacts are taken either by using spring loaded equally spaced sharp probes or by using conducting silver epoxy. For better stability of the electrical measurements using silver epoxy, a thin layer of gold was initially deposited on oxide films prior to any use of silver epoxy, which act as contact electrodes.

Four probes resistivity measurement:

Four probe electrical characterizations techniques are used for the measurement of various electrical properties of metal oxide thin films such as resistivity (ρ), carrier concentration, carrier mobility, hall coefficients etc.

Electrical resistivity and correction factor of Cu thin films

The sheet resistance and resistivity of thin films were measured using a physical quantity measurement system (PQMS) from Qazar Tech. The probes were placed at the centre of

the films with a probe-spacing of 2 mm. Outer two probes were used for sourcing current (I) and the inner two were used to measure the voltage drop (V) across the surface.

In order to exclude any kind of ambiguity during the resistivity measurement of thin copper oxide films and their further relative comparison, the effect of various correction factors are also tested with metallic Cu films. Various correction factors in thin film resistivity include different film thickness (F_1), geometric dimension (F_2) and the position of the probe near the edge of the samples (F_3). Relation between the resistivity and the correction factors for thin films ($t<<s$) are as follow:

$$\rho\ (s,\tau) = 2\pi s\ (F_1F_2F_3)\ (V/I),$$

where, s is the probe spacing, t is the thickness of the sample and τ is defined as t/s. I-V plots for Cu sample surface show very much liner which is quite obvious for a metal film [Figure 3.25(a)]. The slope of this plot represents the sheet resistance. However, a liner increase in sheet resistance with temperature increase is also observed as shown in Figure 3.25(b).

Now, to study the edge effect related correction factors in 4-probe measurement, different types of rectangular geometry (2.5cm × 4.2cm and 2.5cm × 3cm and 2.5cm × 2.6 cm) of thin Cu films have been considered for the I-V measurements. The rectangular geometry of Cu film is shown in Figure 3.26(a), where film thickness $t < s/2$, a = 2.5cm and b varies from 7.5 to 3.0 cm [54]. *Smits formula* [52] for the rectangular geometry correction factor has been used here as given below:

$$\rho = G\ (V/I) \text{ and } G = (\pi/\ ln2)\ t\ R_1\ (b/s,a/b)$$

where, $\pi/\ ln2$ is equal to 4.5324 for the geometric correction factor of an infinitely large slice of film of thickness $t << s$ and $R_1(b/s,\ a/b)$ is the additional correction factors, applied in case of rectangular geometry [55]. Detailed analyses of the shape and thickness dependent correction factors have been discussed by *Haldor Topsqe* [55]. Generally, F_1 (thickness correction factor) and F_3 (edge correction factor) were considered for the non-conducting substrates which is well suited with our case of glass substrates. Here, our motivation was to verify the F_1 and F_3correction factors for thin Cu films for different rectangular shapes (2.5cm × 4.2cm, 2.5cm × 3cm and 2.5cm × 2.6cm) and finally confirm that for a sufficiently large film surface, this factor (G) will not contribute differently for different copper oxide films.

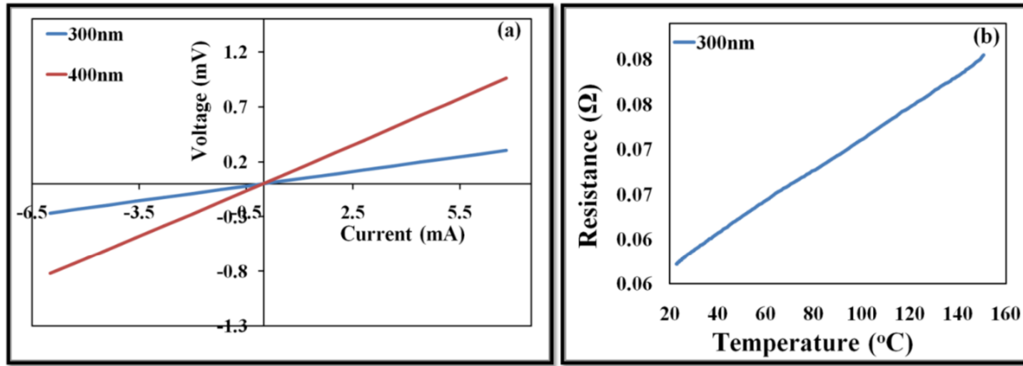

Figure 3.25: *Sheet resistance of thin Cu films (a) I-V plot at room temperature (b) R-T Plots.*

From the results of Figure 3.26(b), it is quite clear that the sheet resistance increases with the decrease of the rectangular geometry (from 2.5cm × 4.2 to 2.5cm × 3.0cm) of the Cu films. Figure 3.26 (c) represents the rectangular correction factors R_1 of Cu film for a particular thickness (~350 nm) by varying the probe position near the edge of the surface. The R_1 correction factor increases with the increase of the rectangular geometry and finally saturates for large film surface. This is good agreement with the reported literature [54, 56] and also excludes any ambiguity during the resistivity measurements of different copper oxide films.

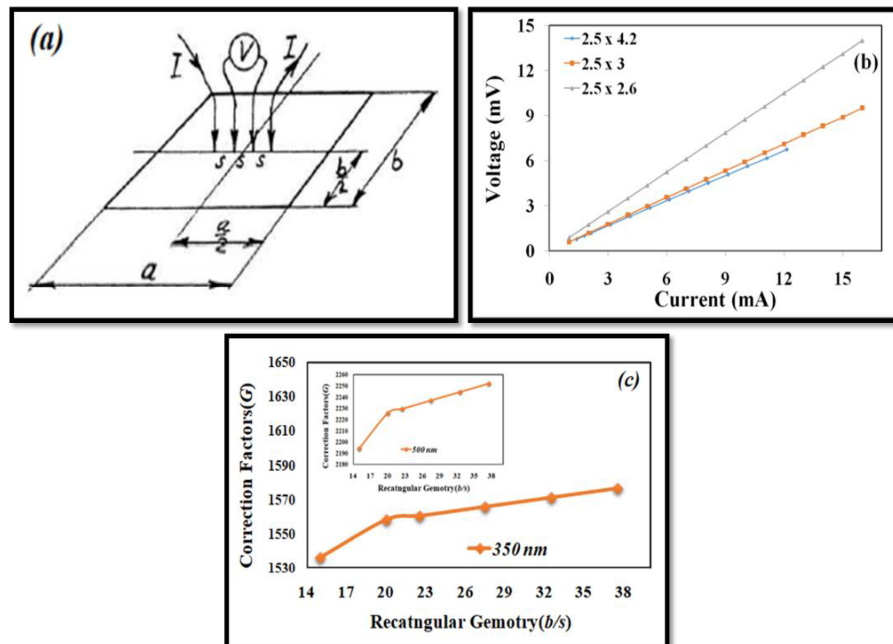

Figure 3.26: *(a) Rectangular geometry of thin Cu film (t < s/2, a = 2.5cm and b varies from 7.5 to 2.6 cm) (b) Sheet resistance and(c) G correction factor for thin Cu films of different rectangular geometry as a function of probe spacing (s/b).*

Electrical resistivity (I-V) measurement

In this part the effect of oxidation temperature and duration on the electrical transport properties of nano-structured CuO thin films is discussed. Surface resistance of thin CuO films is measured in two ways. Either by a four spring loaded linear probe setup or using Au contact electrodes deposition followed by silver epoxy. A schematic of this Au contact electrodes for surface resistance measurement is depicted in Figure 3.27. Any two of this Au contact are used for the I-V measurement keeping the same geometric factor for all samples. A KETHLEY 2400 source meter is used to measure the current voltage (I-V) characteristics of thin CuO films which are later used as sensing materials for CO sensors.

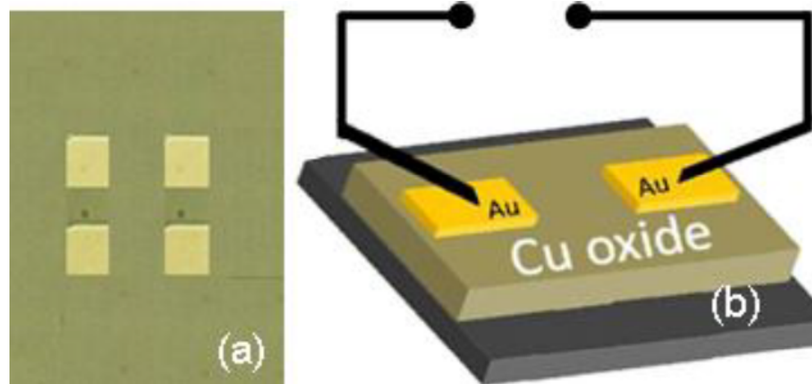

Figure 3.27: *Schematic representation of the surface electrical resistivity (I-V) measurement (a) top view and (b) cross-sectional view.*

I-V characterization of thin CuO films grown at different oxidation temperatures and durations are presented in Figure 3.28. As shown in Figure 3.28, all I-V plots show a linear response and pass through the origin. This finding suggests an ohmic response, having voltage independent constant resistance for each CuO samples. Figure 3.29 represents the RT plot of CuO films grown by oxidation at different temperature for 4 hr and 6hr. The highest sheet resistance of the CuO film is observed for CuO sample oxidized at lower temperature (350°C) and it decreases steadily with higher oxidation temperature. A comparative study between 6hr and 4hr of oxidation has also been performed which suggests that the longer oxidation can also lead to a decrease in surface resistance significantly. For both cases, surface resistivity of the CuO film steadily decreases with the oxidation temperature and moves towards a stable value at about

600°C as can be seen in Figure 3.29. A very similar kind of decrease in CuO sheet resistivity for higher oxidation temperature has also been reported by *Valladares et al.* [32] and *Figueiredo et al*. [34].

The resistance of the CuO film prepared at 350°C appears highest because of large amount of defects and dislocations within the film due to limited thermal diffusion. Resistivity of these films is significantly lowered for higher oxidation temperature due to an enhanced thermal mobility of the oxide atoms. This will significantly influence on formation of larger CuO grains at higher oxidation temperatures. Since the sizes of crystalline grains contribute to defining the electrical resistance of a material, grain size is considered to be a significant factor that controls the surface resistance of CuO thin films. This can be explained by "grain boundary model" in terms of electrical conduction and charge transport in polycrystalline thin films, which is based on the flow of the majority and minority charge carriers [52, 54-55]. The crystallites size is directly observed from active surfaces area (spread out) of thin films [55]. It can be explained in such a way that as average diameter of the crystallites is increased with the oxidation temperature. This will further decrease the carrier scattering at the grain boundaries by increasing the active surfaces area for carrier transport [50].

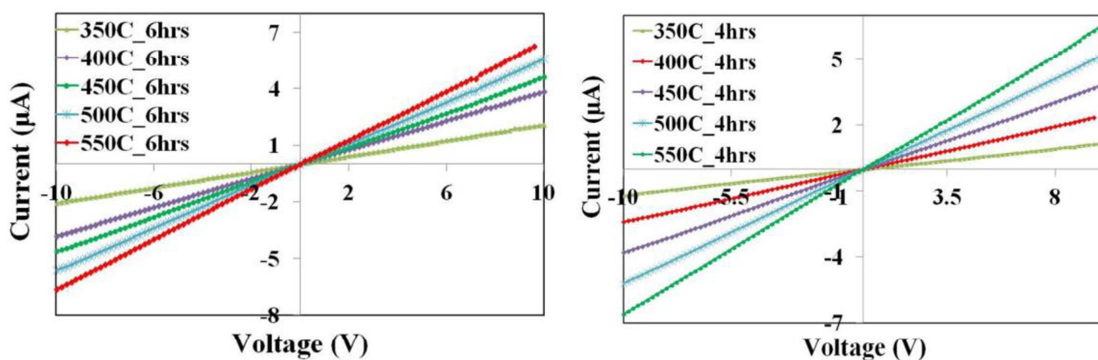

Figure 3.28: *Surface electrical resistivity (I-V) measurement of CuO films grown at different temperatures for duration of (4hr and (b) 6hr.*

In general, CuO shows a p-type nature even without any doping element. This effect is largely due to the presence of unintentional Cu vacancy within the oxide layer which leads to the formation of holes as a majority carrier. However, carrier

concentration and mobility can significantly influence the resistivity of CuO films surface. Basically, the presence of copper vacancies in CuO thin films is the key feature behind the p-type nature of this oxide which exhibits a very close impact with the oxidation temperature. It is expected that at higher oxidation temperature, outer diffusion of Cu atom as well as inner diffusion of O_2 atoms are facilitate during the surface oxidation process of thin Cu films. As a consequence it will further lead to the stoichiometric issue of CuO with an enhanced Cu vacancy within the oxide layer. As a result, a higher carrier (hole) concentration is achieved for oxidation at higher temperature. Therefore, oxidation temperature can significantly alter the carrier (hole) concentration of the CuO film and hence the surface resistance. Moreover, stronger diffusion of free charge carriers and larger oxide grains at higher temperature can promote a faster carrier mobility of the CuO film [57].

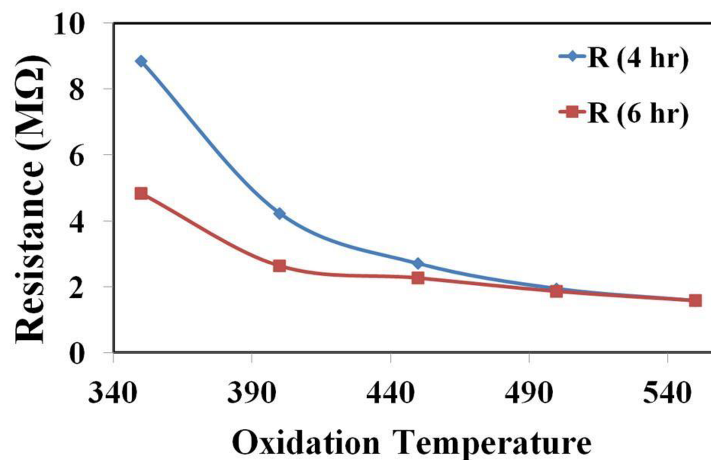

Figure 3.29: *Comparison of the surface electrical resistivity measurement of CuO thin films for different oxidation temperatures.*

Hall Effect

In addition, Hall measurement of these samples using Van der Pauw method has also been performed using silver epoxy to get the informations about carrier concentration and their mobilities. A comparison of sheet and bulk resistivity, carrier (hole) concentration and hole mobility of CuO films, grown at different oxidation temperatures are shown in Table 3.5. Similar to I-V measurements, both sheet and bulk resistivity are significantly decreased with oxidation temperatures. A clear increase in hole

concentration is also observed whereas a decrease in hole mobility can also be found. Increase in hole concentration with oxidation temperature can be related to the Cu vacancy model. However, the drop in carrier mobility may be related to the mutual scattering of the carriers due to their enhanced concentration. However, all these findings finally result in a decreased surface resistance for CuO films oxidized at relatively higher temperature. It has to be taken in to account that further increase in oxidation temperature beyond 600°C may cause an outer diffusion of O_2 atoms from the oxide species. As a result, an increase in the surface resistivity is also expected above 800°C which has also been reported for CuO films [32].

Table 3.5: *Hall data of CuO films, grown at different oxidation temperatures.*

Sample no. (growth temp)	Carrier type	Resistivity (Ω-cm)	Hall Mobility (cm^2/V-s)	Carrier (hole) concentration (cm^{-3})
(I) 350°C@9h	p	0.053	173	6.8×10^{18}
(II) 500°C@9h	p	0.047	60	22.1×10^{18}
(III) 600°C@6h	p	0.031	1.16	1728.9×10^{18}

3.4 APPLICATIONS OF COPPER OXIDE THIN FILMS

3.4.1 Photo catalytic Activity of Cu_2O thin film

As discussed in privies Chapter, the photo catalytic activities of nano-structured Cu_2O thin film (oxidized at 320°C for 3hrs) is studied using methylene blue (MB), an industrial dye in textile industry. Methylene blue (MB) is a cationic dye used extensively for dying cotton, wool and silk. Disposal of this dye in waste water may raise the risk of eye burns, nausea, vomiting and diarrhea [58-59] if this water is anyhow used. Approximately 20% of the overall dye production of the world is discharged from various industries such as dyestuff manufacturing, dyeing, printing, and textile finishing [59-60]. In this research work, degradation of MB as a dye pollutant is investigated in the presence of visible light using Cu_2O thin films as photo-catalytic layer. Details study of preparation of MB dye solution as well as the photo catalytic dye-degradation process under visible light is already discussed in Chapter 2.

The photo catalytic degradation of MB using Cu_2O thin film as catalyst under visible light is performed at room temperature (RT). The degradation kinetics of MB is estimated by a UV-visible spectroscopy. The characteristic absorption of MB at a

wavelength of 664 nm is observed for photo catalytic degradation process [12, 61] when the whole reaction is maintained in darkness. The decrease of absorbance for the samples at λ_{max} after irradiation in a desired time interval represents the rate of decolonization [Figure 3.30] [12].

Figure 3.30(a) shows the UV-vis absorption spectra of MB dye solution with nano-structured Cu_2O thin film as a photo catalyst for various durations (0-15min). Initially, the catalytic surface (Cu_2O thin film) does not show any degradation but after 3 min, MB decomposition starts under visible light irradiation. The absorption decreases rapidly with increases in exposure time from 0 min to 15 min and completely disappears after 15 min. The dark blue color of MB dye solution is gradually lightened during the photo-degradation process as the exposure time is extended. Therefore, it can be concluding that catalytic Cu_2O nano-structured thin film shows an excellent photo catalytic activity and successfully degrade the MB solution under visible light irradiation.

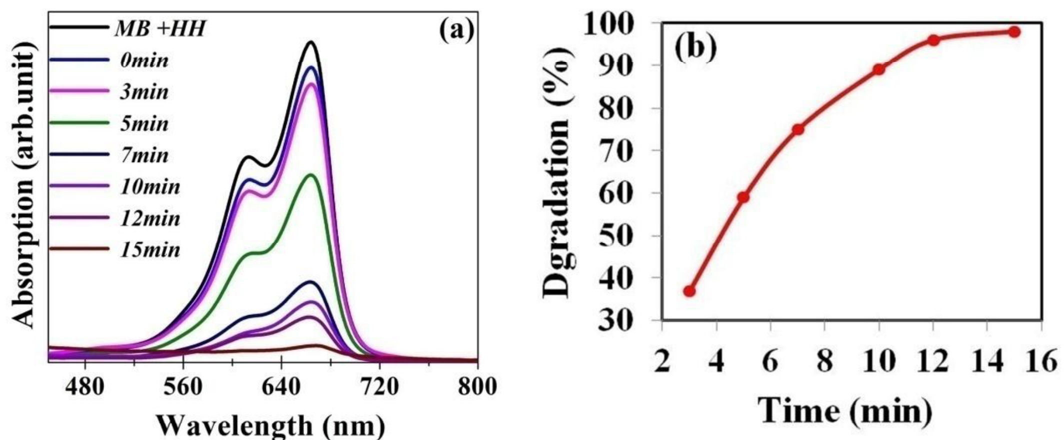

Figure 3.30: *UV-Vis absorption spectra and (b) MB dye degradations with irradiation time for nano-structured Cu_2O thin film under visible light.*

Figure 3.30(b) shows the result for MB dye degradations process with visible light irradiation time using nano-structured Cu_2O thin film. It is clearly identified that as a photo catalyst, nano-structured Cu_2O thin film exhibit 98% degradation of MB (2×10^{-4} M concentration) within 15 min under visible light. In general, a large number of surface charges involve in the photo absorption and emission processes for Cu_2O thin film. In addition, the excess number of Cu vacancy sites enhances the efficiency of photo catalytic process. When the dye solution of MB is exposed to visible light in presence of

catalysis, the $^1Dye_o^-$ molecules are excited to first excited singlet state ($^1Dye_1^-$). These excited molecules are then transferred to the triplet state. On the other hand, initially the electron (e^-) and hole (h^+) pairs are generated by SMO due to the absorption of photons. The OH^- will react with hole (h^+) of the SMO to generate OH radicals, which convert the dye molecules into colorless. The participation of OH radicals as an active oxidizing species was confirmed by carrying out the same reaction in presence of some hydroxyl radical scavengers, where the rate of degradation was drastically reduced [62]. Similar type of research has also been reported for TiO_2 thin films [12].

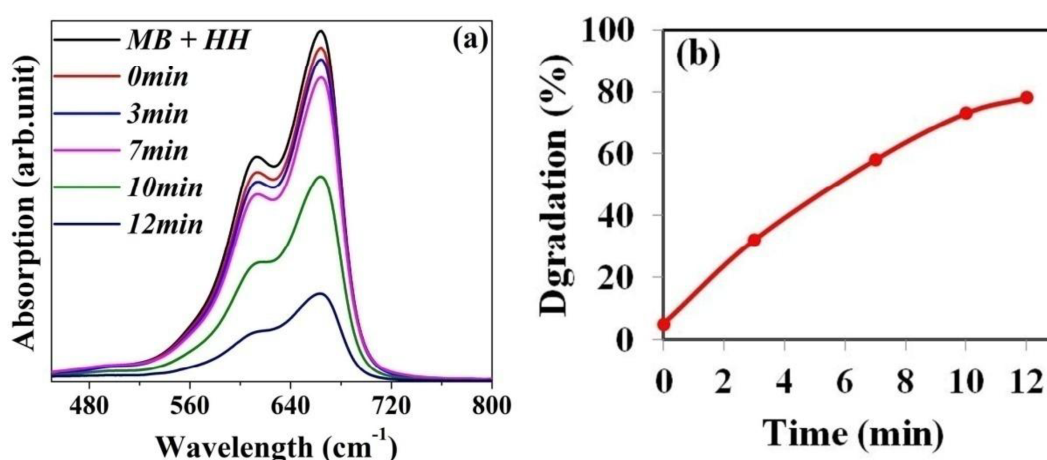

Figure 3.31: *(a) UV-Vis absorption spectra and (b) MB dye degradations with irradiation time for nano-structured CuO thin film under visible light.*

To compare the photo-catalytic activity of CuO thin film with Cu_2O films, similar dye degradation process has been followed for CuO thin film. The CuO films used here was grown by 3hrs of oxidation of Cu films at 350°C and exhibits a granular surface morphology. Figure 3.31(a) show the absorption spectra whereas Figure 3.31(b) represents MB dye degradation after different irradiation time for nano-structured CuO thin films under visible light. It can clearly be observed that CuO thin film exhibit only 70% degradation of MB dye within 12 min under the visible light. This finding indicates that Cu_2O film appears to be superior over the CuO film as photo-catalytic dye degradation. This is mainly due to the indirect band gap of CuO, with much smaller energy bandgap of 1.3eV -1.5 eV lies in the infrared region.

3.4.2 CO sensing of CuO thin films

In this work nano-structured CuO thin films are used as sensing surface whereas dry CO is used as a sensing gas. Three different CuO films denoted as **Sample-I**, **Sample-II** and **Sample-III** were used as CO sensor and their sensing performances have been compared. These three samples were prepared by oxidation of thin Cu films at **(I) 350°C for 9hrs**, **(II) 500°C for 9hrs** and **(III) 600°C for 6hrs**, respectively. These CuO thin films are having a very distinct surface morphology which is already discussed in FESEM result. In addition, their electrical properties are found to be quite different as discussed earlier. Operating temperature for these CuO based CO sensors is varied from 150°C to 300°C. A very low concentration of CO, staring from 25 *ppm to* 320 *ppm* has been tested here. Details of CO sensing set up as well as CuO sample preparations, sensing process and performance are well described in Chapter 2.

Within this set up,CO gas sensing responses are measured ina dynamic gas flow mode where the response is defined as R_{gas}/R_{air}. Here, R_{gas} and R_{air} are the resistance of the sensor in presence of CO gas and in air, respectively. A typical time dependent surface resistance of a CuO thin film based sensor upon exposure of CO gas for various concentrations (25ppm to 320ppm) in dry air is shown in Figure 3.32(a). CuO films are generally verified as of p-type semiconducting behavior of metal oxide. Figure 2.30 shows that the air ambient surface resistance rapidly increases and reaches a maximum value (near plateau) upon exposure of CO gas. This mechanism can be explained in terms of the adsorption/desorption reactions of CO molecules on the surface of thin CuO films. When p-type CuO surface with holes as majority carrier is exposed to dry air, oxygen molecules are adsorbed on its surface to produce oxygen ions (O^{2-}, O^{-}, or O_{2-}) by capturing free electrons from the surface of CuO film.

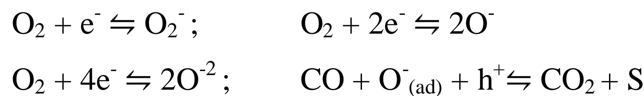

$$O_2 + e^- \leftrightharpoons O_2^- ; \qquad O_2 + 2e^- \leftrightharpoons 2O^-$$

$$O_2 + 4e^- \leftrightharpoons 2O^{-2} ; \qquad CO + O^-_{(ad)} + h^+ \leftrightharpoons CO_2 + S$$

This capture of electrons leads to an relative increase in hole concentration near the CuO surface and as a result surface resistivity drops. During CO (reducing gas) exposure, the pre-absorbed ionized oxygen species on film surface react and release back the absorbed electron which further recombine with holes and results in a decreased in hole concentration. As a result, the resistance of the CuO-based sensor increases upon exposure with CO gas [64- 69].Therefore, increase in surface electrical resistance in the

presence of CO gas confirming the p-type nature of the CuO film. In addition, how efficiently a sensor can response with a test gas exposure is determined by its response and recovery times. These values are calculated from the time taken to achieve the 90% change of the surface resistance during addition or removal of the test gas, respectively. A schematic of response and recovery times is presented in Figure 3.32(b).

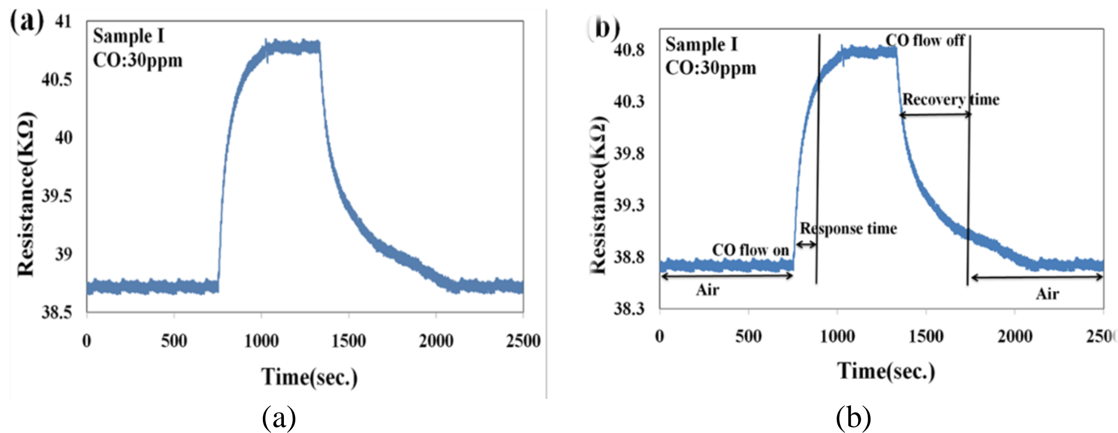

Figure 3.32: *(a) p-type semiconducting behavior and (b) a schematic of response and recovery times of a CuO thin film based sensor in the exposure of CO gas.*

However, the sensor performance of any sensor can largely be affected by the impact of operating temperature and the concentration of the test gas as discussed in the following [Figure 3.33]. Three different CuO sensors are tested here for their sensing performance at various operating temperatures and CO concentrations. Figure 3.33 depicts the sensor response of nano-structured CuO thin films (Sample I, Sample II and Sample III), towards different CO concentrations and as a function of operating temperatures. It is clearly noticed from Figure 3.33 that with increase in operating temperature CO response initially increases and reaches a maximum, afterwards starts to decreases. This finding can be attributed to the temperature dependent adsorption and desorption dynamic equilibrium state. With increase in operating temperature, the adsorbed CO gas attains saturation levels at a suitable temperature (known as optimum operating temperature) and after that the balance of desorption gets disrupted thus causing decrease in gas response [64, 65]. The CO sensing of sample I starts at CO concentration of 25*ppm* and the response reaches a maximum at 230°C [Figure 3.33 (a)], while for sample II, the sensing starts at 30*ppm* with the response maxima at 250°C [Figure 3.33 (b)]. Similarly, sample III exhibits the sensing starts at 50*ppm* and the sensor shows a height response at 280°C

operating temperature [Figure 3.33(c)]. This maximum sensing temperature for a particular sensor is known as the optimum operating temperature (sensor temperature). In all cases, a clear increase in sensing response with CO concentrations are also observed, while keeping the optimum operating temperature same. In addition, the sensing response for a particular CO concentration of 50 ppm, are also compared for all three samples, as depicted in Figure 3.33 (d). Sample I shows a clear superiority in CO sensing over the other two samples.

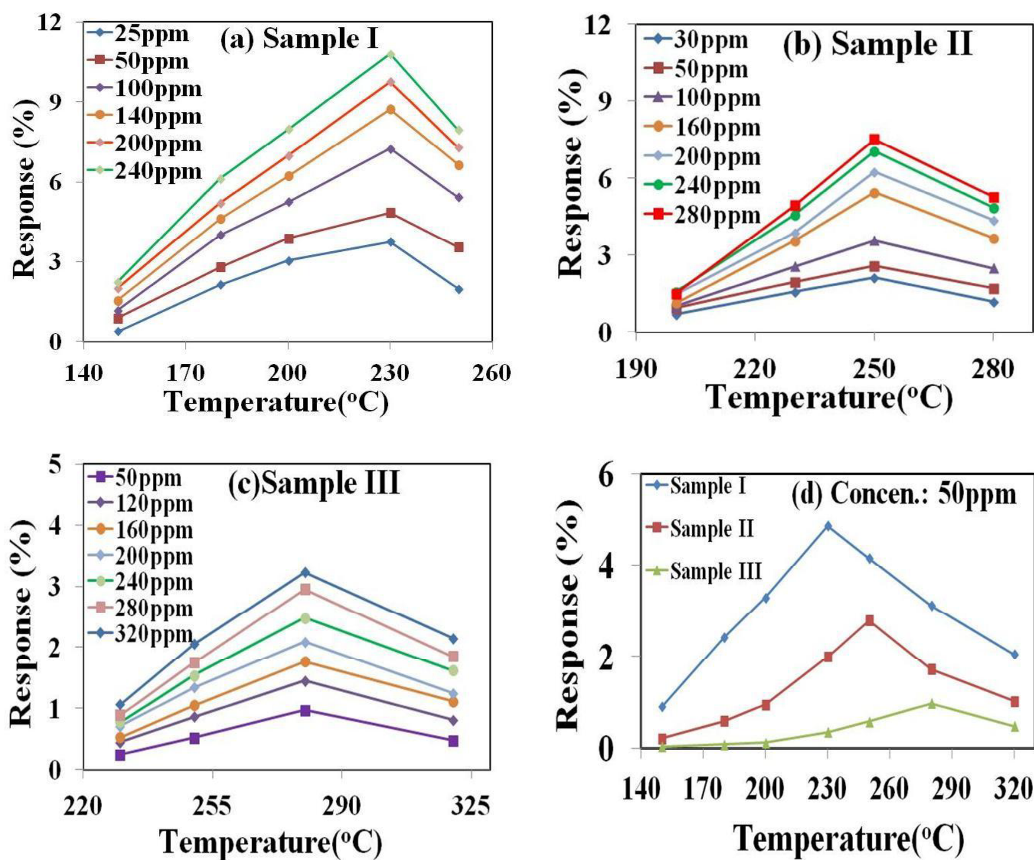

Figure 3.33: *Variation in sensors response of (a) sample I, (b) sample II, (c) sample III for different concentration and at (d) 50ppm of CO gas as a function of operating temperature (150°C to 250°C).*

Time dependent surface resistance of CuO thin films (Sample I, sample II and sample III) based sensor upon exposure of CO gas of various concentrations (25ppm to 320ppm) in dry air are shown in Figure 3.34 (a-c). Here the optimum operating temperatures of 230°C, 250°C and 280°C for sample I, sample II and sample III, respectively are used as operating temperatures. A gradual increase in sensing response

with the CO concentration is clearly observed for all samples up to certain value after that CO response for all samples become saturated. The base resistance of sample I appear to be much higher (39 KΩ) as compare to that of sample II (5.2 KΩ) and so as sample III (3.7 KΩ). These findings are complementary with our earlier electrical measurement (I-V) of CuO films grown at different oxidation temperatures. The optimum operating temperatures for all three CuO based CO sensors samples are also plotted against their oxidation temperature in Figure 3.34(d). An increase in optimum operating temperature with the CuO oxidation temperature is clearly observed. All these finding can be explained in terms of adsorption-desorption kinetics, surface morphology of the CuO sensing layer as well as unintentional Cu vacancy model.

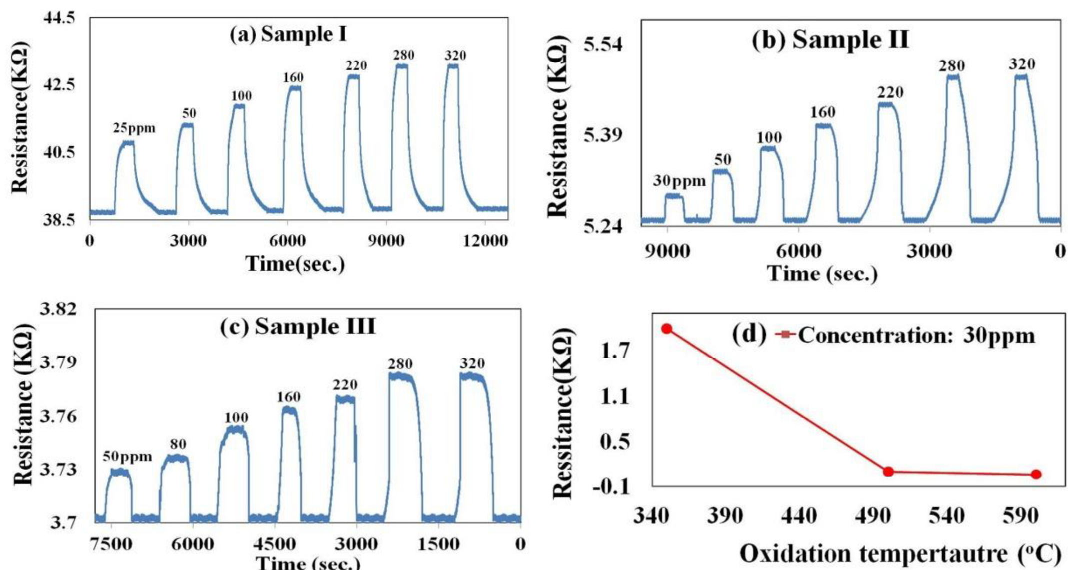

Figure 3.34: *Change in surface electrical resistance due to exposure to various concentrations of CO gas at optimum operating temperatures(a) 230°C for sample I, (b) 250°C for sample II, (c) 280°C for sample III and (d) Sensor operating temperature increases with the oxidation temperatures.*

It is clearly observed that the operating temperature is an important parameter for CuO thin films sensors, which can be explain in terms of absorption and desorption of oxygen on the oxide surface (discussed in chapter 2). Moreover, the operating temperature also decides the power dissipated by heater to find the optimal gas sensing characteristics. Here, sample I based sensor provides the best results among all three. The sensing efficiency of CO gas starts with minimum concentration of *25ppm*as well asit works at lowest optimum operating temperature of 230°C. Both observations

indicate the sensing superiority of sample I over sample II and sample III based sensors. The lower operating temperature is one of the most desired criteria for any sensor to minimize the power consumption. In addition, a low operating temperature is also preferred for any sensor due to safety reason when it works in an open atmosphere ambient. In one hand, the operating temperature can be reduced by optimizing the morphological geometry of the sensing layer. On other hand, this can be achieved by modulating the electronic properties of the sensing material either by proper doping or special treatment.

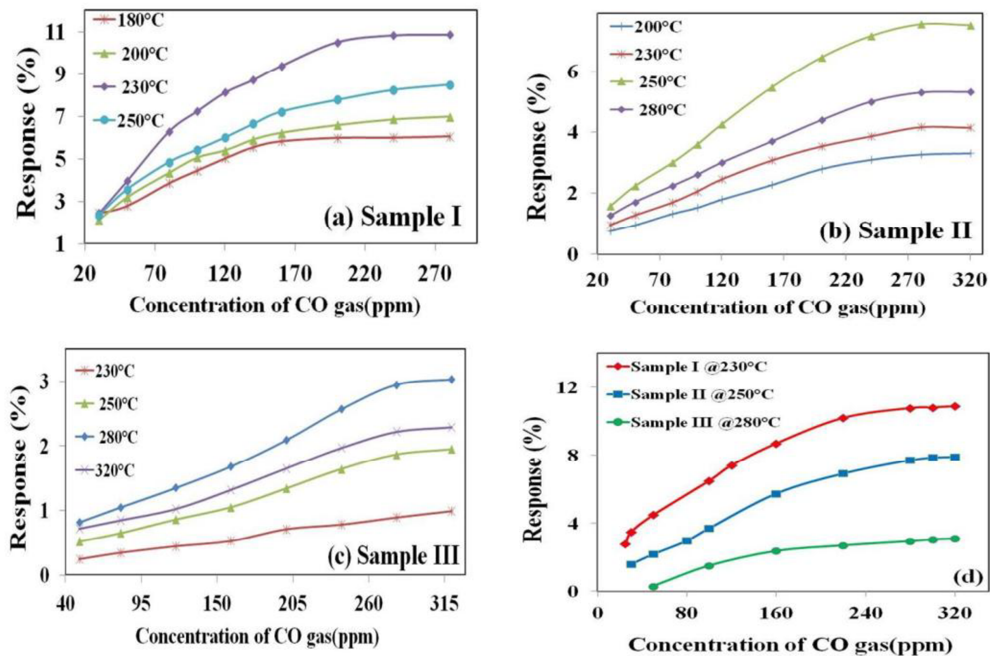

Figure 3.35: *The sensors response for different operating temperatures as a function of CO concentration for (a) sample I, sample II, (c) sample III and (d) at optimum operating temperatures for all nano- structured CuO thin films based sensors.*

Figure 3.35 represents the CO response for sample I, sample II and sample III as a function of CO concentration (25-320 ppm) for different operating temperatures. It is clearly observed for all sensors that the response has a trend to increase with initial CO concentration. Initially, the response increases sharply up to certain CO concentration and become saturated. Afterwards, the change in the sensor response is insignificant. However, for each samples, highest response is found for the optimum operating temperatures of 230°C, 250°C and 280°C, respectively. This can also be observed from Figure 3.35 (d) that relationship between sensor response and CO concentration is almost linear up to about 180ppm, 220ppm and 240ppm, respectively for sample I, sample II

and sample III, sensing at their optimum operating temperatures. In fact, the response of the SMO sensor can usually be expressed as

$$S = A[C] N + D$$

where,A and D are constants and C is the concentration of the target gas. N depends on the surface charge and the stoichiometry of the sensing materials and usually ranges between 0.5 to 1.0 [64, 70]. During absorption of CO molecules on CuO surface, they form bonds by donating and σ-electron to the metal ion (Cu^{+2}) and a reverse donation of π-electrons to CO is occurred. With increase in CO concentration, adsorption and reaction processes at the Cu sites enhance the sensing response. A similar type of CO reactivity has also been reported for the Cu:ZnO thin film based CO sensor [71-72].

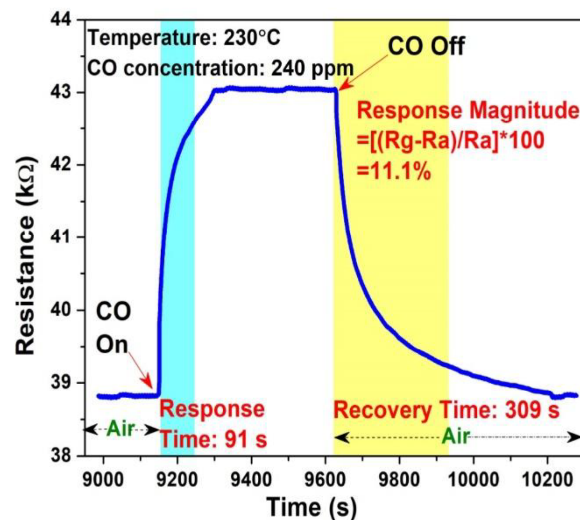

Figure 3.36: *Transient behavior of the CuO sensor at optimum temperature (230°C) and 240 ppm indicating response magnitude, response time and recovery time.*

It can clearly be observed from Figure 3.35(d) that maximum response with minimum concentration (25pppm - 30ppm) is obtained from sample I at 230°C operating temperature. Whereas, sample II and sample III can sense the CO gas at 30ppm and 50ppm of their optimum operating temperate, respectively. This effect can be explained in two ways. Firstly, the surface area to volume ratio of the CuO film, hence the gas accessibility, which can explain the enhanced CO response for sample I. Other option could be the surface charge (carrier) density or carrier concentration of CuO film. Therefore, a combined mechanism of an increased surface adsorption sites

as well as a reduced surface carrier concentration may lead towards the optimum performance of a sensor with am extremely highly sensitivity.

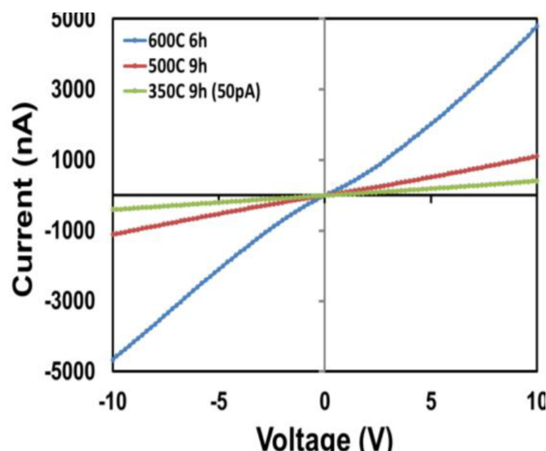

Figure 3.37: *Surface electrical resistivity (I-V) measurement of CuO sensor samples grown at different oxidation temperatures.*

The response and recovery times of CuO based CO sensor are also calculated for sample I, operating at optimum operating temperature of 230°C [Figure 3.36] The CO concentration for sample I was maintained at 240 ppm and a response and recovery time of 91 s and 309 s, respectively, are found. With an appreciable fast response and recovery time, CuO sensor shows a very stable baseline as well as a complete recovery in absence of any CO exposure [Figure 3.36].

To further understand the CO sensing superiority of sample I over other samples, theirs surface morphologies and surface electrical properties are also compared. Sample I shows a rough surface morphology with many tiny granular island [Figure 3.13(d)] whereas other two appear with much larger CuO grains of relatively smoother surface. This finding clearly indicates a larger adsorption sites for CO on sample I as compared to II and III. The surface resistivity (I-V) measurements also suggest a drastically higher baseline resistance for sample I at room temperature with respect to other two [Figure 3.37]. Hall measurement also supports this finding with a reasonable lower carrier (hole) concentration for sample I. Therefore, both these mechanisms significantly enhance the CO sensitivity and finally make CuO film grown at 350°C an efficient CO sensor with fast response and recovery. Moreover, the operating temperature for this CO sensor is as low as 150°C with a sensing limit of as low as 25ppm.

3.5 SUMMARY

Thin films of single oxide phase of copper have successfully been grown on glass and silicon substrates by controlled thermal oxidation of vacuum deposited thin copper films. Sharp XRD patterns suggest the formation of highly crystalline films of copper oxides. Oxidation process of the Cu film is found to be highly sensitive to the diffusion kinetics. However, after sufficient duration of annealing (25 hr), final Cu oxide phase is found to be determined by the oxidation temperature. This finding can be treated as thermodynamic equilibrium. Within the saturation limit, the completion of the oxidation process is mostly controlled by the diffusion kinetics (annealing duration) which further depends on the thickness of initial Cu layers. At a lower oxidation temperature range (250°C - 320°C) crystalline phase of Cu_2O is formed in air ambient condition whereas for higher oxidation temperature of 330°C onwards CuO phase starts to form. Within the range of diffusion limit, longer duration of annealing can leadto the completion of the transformation process of Cu_2O into the CuO phases. In case of single oxide phase of Cu_2O, faceted surface morphology of Cu_2O films, directed by its materialistic properties is observed in SEM images. In addition, Raman and photoemission spectroscopy also confirm the oxide phase purity for both cases. Finally, an optical band gap of about 2.2 eV for Cu_2O films has been observed, makes it a visible light active material suitable for the photo catalytic applications. In addition, the formation final oxide state is also strongly influenced by the O_2 partial pressure. During annealing under oxygen ambient condition, surface oxidation starts at slightly lower oxidation temperature as compared to air ambient. The formation of crystalline Cu_2O phase is found between 140°C-270°C, whereas the CuO phase starts to appear only above 280°C. Within a narrow oxidation temperature window strong growth asymmetry and formation of CuO nano-rods has also been observed both in air as well as under oxygen ambient conditions. All these findings are explained in terms of surface thermodynamic and diffusion kinetics as well as chemical energy.

Present study indicates that single oxide phase, nano-structured thin films of Cu_2O and CuO can be achieved through a simple thermal oxidation method which is further used for photo-catalytic activities such as dye (MB) degradation as well as CO sensing at relatively lower temperature with high sensitivity. In one hand, Cu_2O thin film has successfully been used for the photo catalytic degradation of MB (an industrial

pollutant) under visible light irradiation. The dye degradation results indicate that the single phase Cu_2O films prepared at 320°C for 3hrs has higher photo degradation efficiency of 98%. On other hand, CuO films have successfully been tested as a CO sensing material at lower operating temperature. Gas sensing results is found to be very much promising for CuO films grown at relatively lower oxidation temperature (350°C). It provides a CO sensing platform with a low operating temperature as low as 150°Cand with a very high sensitivity down to 25 ppm.These findings are explained in terms of surface adsorption possibility (morphology) as well as its surface electrical transport properties (resistivity, carrier concentration etc). Finally, CuO thin film based low ppm CO sensor operating at lower temperature can significantly reduce the power consumption and CO sensing at 25 ppm level with fast response and recovery times is of high practical importance for an early detection of low concentration CO poisoning.

Bibliography

[1] G. Zhou and J. C. Yang, Applied Surface Science 222 (2004) 357.

[2] C. L. Chu, H. C. Lu, C. Y. Lo, C. Y. Lai and Y. H. Wang, Physica B 404 (2009) 4831.

[3] S. H. Mohamed, M. E. Hagary and M. E. Ismail, Journal of Physics D- Applied Physics 43 (2010) 075401.

[4] S. Choudhary, J. V. N. Sarma, and S. Gangopadhyay, AIP Conference Proceeding 1724 (2016) 020116.

[5] T. Schmidt, J. I. Flege, S. Gangopadhyay, T. Clausen, A. Locatelli, S. Heun and J. Falta, Physics Review Letter 98 (2007) 66104.

[6] S. Brittman,Y. Yoo, N. P. Dasgupta, S.I Kim, B. Kim and P. Yang, Nano Letters 14 (2014) 4665.

[7] Z. H. Lu and D. Grozea, Applied Physics Letter 80 (2002) 255.

[8] J. Pal, M. Ganguly, C. Mondal, A. Roy, Y. Negishi and T. Pal, Journal of Physics and Chemistry C 117 (2013) 24640.

[9] L. Xiong, F. Yang, L. Yan, N. Yan, X. Yang, M. Qiu and Y. Yu, Journal of Physics and Chemistry of Solids 72 (2011) 1104.

[10] P. Shahbazi, A. Kian, Internal journal of hydrogen energy 4 1 (2 0 1 6) 1 7 2 4 7.

[11] W. Zhang, X. Li, Z. Yang, X. Tang, Y. Ma, M. Li, N. Hu, H. Wei and Y. Zhang, Nanotechnology 27 (2016) 265703.

[12] P. Sangpour, F. Hashemi and A. Z. Moshfegh, Journal of Physics and Chemistry C 114 (2010) 13955.

[13] Z. A. C. Ramli, N. Asim, Wan N. R. W. Isahak, Z. Emdadi, N. A. Ludin, M. A.Yarmo and K. Sopian, The Scientific World Journal 415136 (2014).

[14] M. Yurddaskal, T. Dikici and E. Celik, Ceramics International 42 (2016) 17749.

[15] C. W. Runyan, R. M. Johnson, J.Yang, A. N. Waller, D. Perkis, S. W. Marshall, T. C. Beasley and k. S. McGee, American Journal of Preventive Medicine 28 (2005) 102.

[16] Recommendations for Occupational Safety and Health: Compendium of Policy Documents and Statements U.S. Department of Health and Human Services Public Health Service Centers for Disease Control National Institute for Occupational Safety and Health DHHS (NIOSH), USA, pp. 533-8287, (1992).

[17] L. Armelao, D. Barreca, M. Bertapelle, G. Bottaro, C. Sada and E. Tondello, Thin Solid Films 48 (2003) 442.

[18] T. Kosugi, and S. Kaneko, Journal of American Ceramic Society 81 (1998) 3117.

[19] M. Yang and J. J. Zhu, Journal of Crystal Growth 256 (2003) 134.

[20] S. Heiroth, R. Ghisleni, T. Lippert, J. Michler and A. Wokaun, Acta Mater 59 (2011) 2330.

[21] K. Amikura, T. Kimura, M. Hamada, N. Yokoyama, J. Miyazaki and Y. Yamada, Applied Surface Science 254 (2008) 6976.

[22] S. B. Ogale, P. G. Bilurkar, N. Mate, S. M. Kanetkar, N. Parikh and B. Patnaik, Journal of Applied Physics 72 (1992) 3765.

[23] V. F. Drobny and D. L. Pulfrey, Thin Solid Films 61 (1979) 89.

[24] S. Izhizuka, S. Kato, T. Maruyama and K. Akimoto, Japanese Journal of Applied Physics 40 (2001) 2765.

[25] M. H. P. Reddy, A. Sreedhar and S. Uthanna, Indian Journal of Physics 86 (2012) 291.

[26] K. P. Muthe, J. C. Vyas, S. N. Narang, D. K. Aswal, S. K. Gupta, R. Pinto, G. P. Kothiyal and S. B. Sabharwal, Thin Solids Films 324 (1998) 37.

[27] A. Roos, T. Chibuye and B. Karlson, Solar Energy Materials and solar cells 7 (1983) 453.

[28] A. Fujinaka and A. A. Berezin, Journal of Applied Physics 54 (1983) 3582.

[29] L. Wang and M. Tao, Electrochemical and Solid State Letters 10, H248 (2007).

[30] A. K. Mukhopadhyay, A. K. Chakraborty, A. P. Chatterjee and S. K. Lahiri, Thin Solid Films 209 (1992) 92.

[31] R. P. Wijesundera, Semiconductor Science and Technology 25 (2010) 045015.

[32] L. D. L. S. Valladares, D. H. Salinas, A. B. Dominguez, D. A. Najarro, S. I. Khondaker, T. Mitrelias, C. H. W. Barnes, J. A. Aguiar and Y. Majima, Thin Solid Films 250 (2012) 6368.

[33] S. Choudhary, J. V. N. Sarma, S. Pande, S. A. Girard, P. Turban, B. Lepine and S. Gangopadhyay, AIP Advance 8 (2018) 055114.

[34] V. Figueiredo, E. Elangovan, G. Goncalves, P. Barqunha, L. Pereira, N. Franco, E. Alves, R. Martins and E. Fortunato, Applied Surface Science 254 (2008) 3949.

[35] U. Nerle and M. K. Rabinal, IOSR Journal of Applied Physics 5 (2013) 2278.

[36] G. Papadimitropoulos, N. Voirdas, V. Em Vamvakas and D. Davazoglou, Journal of Physics: Conference Series 10 (2005) 182.

[37] J. D. Aiken and R. G. Finke, Journal Molecular Catalysis A 145 (1999) 1.

[38] Sumita Choudhary, Aditya Venikar and Subhashis Gangopadhyay, Controlled Oxidation of Thin Copper Films under Oxygen Ambient, “AIP Conference Proceedings” (2019) (accepted).

[39] J. Liang, N. Kishi, T. Soga, T. Jimbo and M. Ahmed, Thin Solid Film 520 (2012) 2679.

[40] J. F. Xu, W. Ji, Z. X. Shen, W. S. Li, S. H. Tang, X. R. Ye, D. Z. Jia and X. Q. Xin, Journal of Raman Spectroscopy 30 (1999) 431.

[41] L.S. Huang, S. G. Yang, T. Li, B. X. Gu, Y. W. Du, Y. N. Lu and S. Z. Shi, Journal of Crystal Growth 260 (2004) 130.

[42] Z. H. Gan, G. Q. Yu, B. K. Tay, C. M. Tan, Z. W. Zhao and Y. Q. Fu, Journal Physics. D: Applied Physics 37 (2004) 81.

[43] F. A. Akgul, G. Akgul, N. Yildirim, H. E. Unalan and R. Turan, Materials Chemistry and Physics 147 (2014) 987.

[44] A. P. Litvinchuk, A. Moller, L. Debbichi, P. Krüger, M. N. Iliev and M. M. Gospodinov, Journal of Physics Condensed Matter 25 (2013) 105402.

[45] D. Jundale, S. Pawar, M. Chougule, P. Godse, S. Patil, B. Raut, S. Sen and V. Patil, Journal of Sensor Technology, 1 (2011) 36.

[46] J. Ghijsen, L.H. Tjeng, J. van Elp, H. Eskes, J. Westerink, G.A. Sawatzky and M.T. Czyzyk, Physical Review B 38 (1988) 11322.

[47] D. Tahir and S. Tougaard, Journal of Physics, Condensed Matter 24 (2012) 175002.

[48] D. Barreca, A. Gasparotto and E. Tondello, Surface Science Spectra 40 (2007) 41.

[49] K. Khojier, H. Savaloni and Z. Sadeghi, Journal of Theoretical Applied Physics 8 (2014) 116.

[50] C. D. Wagner, L. E. Davis, M. V. Zeller, J. A. Taylor, R. M. Raymond and L. H. Gale, Surface and Interface Analysis 3 (1981) 211.

[51] D. Barreca, A. Gasparotto and E. Tondello, Surface Science Spectra 40 (2007) 41.

[52] C. Powell and A. Jablonski, NIST Standard Reference Database 71, National Institute of Standards and Technology, Standard Reference Data Program Gaithersburg, Maryland 20899 (2010).

[53] L. M. Wong, S. Y. Chiam, J. Q. Huang, S. J. Wang, J. S. Pan and W. K. Chim, J. Applied Physics 108 (2010) 033702.

[54] S. Choudhary, R. Narula and S. Gangopadhyay, AIP Conference Proceedings 1953 (2018) 100054.

[55] Haldor Topsqe, Geometric factors in four-point resistivity measurement, 2nd Revised Edition, Bulletin No. 472-13, File no. 472, Semiconductor Division (1968).

[56] F. M. Smits, The Bell System Technical Journal 37 (1958) 711.

[57] S. L. Patel, S. Chander, A. Purohit, M.D. Kannan and M.S. Dhaka, Journal of Physics and Chemistry of Solids 123 (2018) 216.

[58] H. I. Abdulgafour, Y. Yusof, F.K. Yam and Z. Hassan, Advance Materials Research 620 (2013) 132.

[59] N. M. Ahmed , F. A. Sabah, H. I. Abdulgafour, A. Alsadig, A. Sulieman and M. Alkhoaryef, Results in Physics 13 (2019) 102159.

[60] M. Oztas, China Physics Letter 25 (2008) 4090.

[61] A.R. Lang, Dyes and pigments: new research, Nova Science Publishers, UK (2013).

[62] A. H. Mahvi, M. Ghanbarian, S. Nasseri and A. Khairi, Desalination. 239, 309 (2009).

[63] M. Salehi, H. Hashemipour and M. Mirzaee, American Journal of Environmental Engineering, 2 (2012) 1.

[64] Z. Shan, W. Wang, X. Lin and H. Ding, F. Huang, Journal of Solid State Chemistry 181 (2008) 1361.

[65] R. Ameta, D. Kumar and P. Jhalora, Acta Chimica Pharmaceutica Indica 4 (2014) 20.

[66] F. I. S. Hasina and S. S. Suryanvanshi, School of Physical Science, Sholapur University, Sholapur, MP (2017).

[67] L. P. Chikhale, J. Y. Patil, A. V. Rajgure, F. I. Shaikh, I. S. Mulla and S. S. Suryavanshi, Measurement 57 (2014) 46.

[68] S. Steinhauer, E. Brunet, T. Maier, G.C. Mutinati and A. Kock, Transducers, (2013) 1095.

[69] C. Wang, X. Q. Fu, X. Y. Xue, Y. G. Wang and T. H. Wang, Nanotechnology 18 (2007) 145506.

[70] P. Shankar, and J. B. B. Rayappan, Journal of Science Letters 4 (2015) 126.

[71] L. Houa, C. Zhanga, L. Lia, C. Dua, X. Lia, X.-F. Kang and W. Chen, Talanta 188 (2018) 41.

[72] M. S. Khandekar, N. L. Tarwal, J. Y. Patil, F. I. Shaikh, I. S. Mulla, S. S. Suryavanshi, Ceramics International 39 (2013) 5901.